

Controlled nonperturbative dynamics of quantum fields out of equilibrium

Jürgen Berges*

Universität Heidelberg, Institut für Theoretische Physik
Philosophenweg 16, 69120 Heidelberg, Germany

Abstract

We compute the nonequilibrium real-time evolution of an $O(N)$ -symmetric scalar quantum field theory from a systematic $1/N$ expansion of the $2PI$ effective action to next-to-leading order, which includes scattering and memory effects. In contrast to the standard $1/N$ expansion of the $1PI$ effective action, the next-to-leading order expansion in presence of a possible expectation value for the composite operator leads to a bounded time evolution where the truncation error may be controlled by higher powers in $1/N$. We present a detailed comparison with the leading-order results and determine the range of validity of standard mean field type approximations.

We investigate “quench” and “tsunami” initial conditions frequently used to mimic idealized far-from-equilibrium pion dynamics in the context of heavy-ion collisions. For spatially homogeneous initial conditions we find three generic regimes, characterized by an early-time exponential damping, a parametrically slow (power-law) behavior at intermediate times, and a late-time exponential approach to thermal equilibrium. The different time scales are obtained from a numerical solution of the time-reversal invariant equations in $1+1$ dimensions without further approximations. We discuss in detail the out-of-equilibrium behavior of the nontrivial n -point correlation functions as well as the evolution of a particle number distribution and inverse slope parameter.

*Email: j.berges@thphys.uni-heidelberg.de

1 Introduction and overview

Current and upcoming heavy ion collision experiments at RHIC and the LHC have been an important motivation for the study of quantum field theory in and out of equilibrium. With these experiments one aims for a Quark Gluon Plasma produced in a transient state, finally releasing high multiplicities of particles of which the lightest hadrons are the pions. One major open question in the description of the underlying physics concerns the justification of current quantum field theoretical predictions based on equilibrium thermodynamics, local equilibrium or linear response assumptions. Immediately related to this appears the question for possible new signatures from processes which are far away from equilibrium. In contrast to a thermally equilibrated state, which keeps no information about the details of the initial conditions, nonequilibrium phenomena may help to understand in particular the earlier stages of a collision.

A successful description of the dynamics of quantum fields away from equilibrium is tightly related to the basic problem of how macroscopic “dissipative” behavior arises from time-reversal invariant quantum dynamics. This is a fundamental question with most diverse applications. The techniques, which have to be developed to understand the physics of heavy-ion collision experiments, will be of relevance to the inflationary dynamics in the early universe, to the physics of baryogenesis or even to nonequilibrium aspects of mesoscopic quantum devices.

The description of nonequilibrium quantum field theory from “first principles” can be based on a path integral formulation using the Schwinger-Keldysh techniques [1]. In analogy to vacuum or thermal equilibrium quantum field theory one can construct a generating functional for nonequilibrium Green’s functions which contains all quantum and statistical fluctuations for given initial correlations or density matrix.

However, controlled computational methods for the approximative solution of time evolution problems which respect the symmetries of the underlying theory are limited so far. In order to understand how macroscopic, effectively irreversible behavior arises one cannot use phenomenological approaches which typically break the time-reflection symmetry of the underlying theory. Simple (finite-loop) perturbative descriptions can be unbounded and are known to break down at late times [2]. While standard nonperturbative methods based on lattice Monte Carlo simulations have been successfully applied to thermal quantum field theory in Euclidean time, a

non-positive definite probability measure at real times already prevents their use. In contrast, classical field theory can be simulated. One only has to solve the classical field equations of motion sampled with the appropriate initial condition. Of course, the latter is not capable of treating genuine quantum effects but it should be reliable when the number of field quanta in each mode is sufficiently large. Another approach to which much work has been devoted restricts the discussion to systems close to thermal equilibrium or to effective descriptions based on a separation of scales in the weak coupling limit. For a recent review of the very interesting developments in this field see Ref. [3].

Away from equilibrium, time-reflection invariant approximations to quantum field theories have been almost uniquely based on mean field type approximations (so-called “collisionless” Hartree (-Fock) or leading order large- N approximations) [4]. It is a known problem that the latter approximations are unable to describe thermalization at late times¹, and their extensive use is based on the assumption that scattering effects may not change the picture dramatically for sufficiently early times. Efforts to go beyond mean field include a $1/N$ expansion of the generating functional for one-particle irreducible ($1PI$) Green’s functions beyond leading order [6, 7]. However, the standard $1/N$ expansion of the $1PI$ effective action turns out to be unbounded in time [7]. For time evolution problems it therefore fails to give a controlled expansion.

Recent progress came from a rather old concept based on a loop expansion of the generating functional for two-particle irreducible ($2PI$) Green’s functions as introduced in Refs. [8, 9, 10, 11]. It has been demonstrated in Ref. [12] for a scalar quantum field theory that a bounded time-evolution can be achieved without further approximations from a three-loop expansion of the $2PI$ effective action. The three-loop approximation reflects all symmetries of the underlying theory and goes beyond the mean field level, including scattering and memory effects. For very different nonequilibrium initial conditions it was shown from a numerical solution in $1 + 1$ dimensions that the three-loop approximation leads to a universal asymptotic behavior of quantum fields. The correlation functions at late time are uniquely determined by the initial (conserved) energy density and approach the equilibrium correlations of the corresponding three-loop thermal field theory [12].

¹For improved results using inhomogeneous mean fields see Ref. [5].

At three-loop order the $2PI$ effective action comprises the classical Boltzmann equation [14, 15, 10, 16, 17, 18]. Without additional approximations the three-loop equations may be viewed as a “quantum Boltzmann equation” including off-shell effects and resumming an infinite order of derivatives [13], which are difficult to include in kinetic descriptions [19, 20]. However, despite the fact that the loop expansion reveals a consistent picture of the early- and late-time physics of quantum fields without further assumptions, in absence of a small expansion parameter it is not a controlled approximation. In this work we will discuss a controlled nonperturbative approximation.

Our aim is to study a quantum field theory which captures aspects of low energy pion physics and which is simple enough that one can perform a quantitative treatment. The basic ingredient for the effective low energy description is the approximate chiral symmetry of the classical action for quantum chromodynamics (QCD). In QCD for N_f flavors the chiral $SU_L(N_f) \times SU_R(N_f)$ is broken to a vector-like $SU(N_f)$, where the pions appear as the corresponding Goldstone bosons. For two flavors the $SU(2) \times SU(2)$ is locally isomorphic to an $O(4)$ symmetry which we will consider in the following. Unlike in chiral perturbation theory we will study here the corresponding *linear* model (“linear sigma model”) for the light scalar and pseudo-scalar degrees of freedom which constitute the $O(N = 4)$ -vector $(\sigma, \vec{\pi})$. For various N this model has been extensively studied in thermal equilibrium, or nonequilibrium as in Refs. [4, 6]².

We employ a systematic **1/N expansion of the $O(N)$ -symmetric 2PI effective action** $\Gamma[\phi, G]$, which does not only depend on a possible expectation value of the quantum field, ϕ , but also on an expectation value of the time-ordered field bilinear, G (cf. Sects. 2, 4). Though $N = 4$ may be used already as an expansion parameter, we will frequently consider larger values of N for the sake of a quantitative treatment. We compute the $2PI$ effective action to next-to-leading order in $1/N$, which goes beyond the mean field-type leading-order approximation and includes scattering and memory effects. This approximation leads to a bounded time evolution for which the truncation error may be controlled by higher powers in $1/N$. In this case the employed expansion provides a **controlled nonperturbative approximation** which is not restricted to the weak coupling regime. Time-

²For $N = 1$ it also describes the long-range fluctuations of the QCD critical point [21].

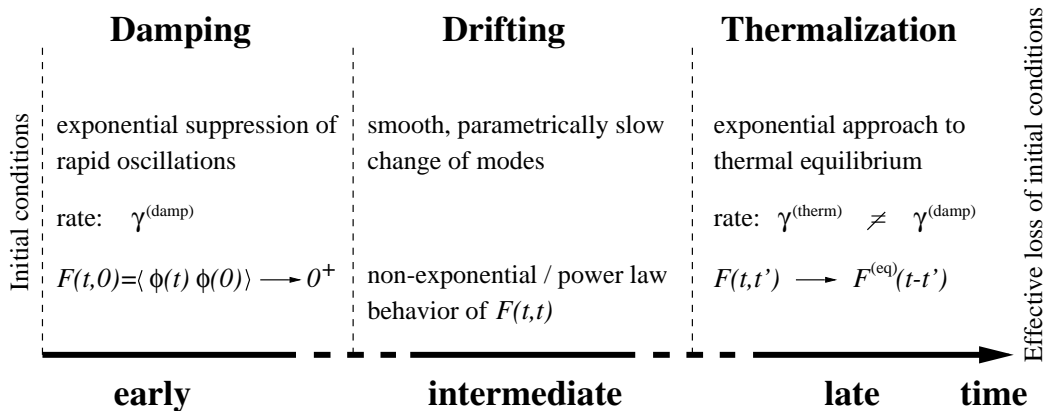


Figure 1: For the $O(N)$ -symmetric scalar theory in 1+1 dimensions we find three generic time regimes: An approximately exponential damping of oscillations characteristic for early times with inverse rate $\tau^{(\text{damp})} \sim 1/\gamma^{(\text{damp})}$, a parametrically slow or power law drifting at intermediate times, and a late-time exponential approach to thermal equilibrium with $\tau^{(\text{therm})} \sim 1/\gamma^{(\text{therm})}$. Both for the employed “quench” and the “tsunami” initial condition $\tau^{(\text{damp})} \ll \tau^{(\text{therm})}$. None of the described different time scales are captured in the standard leading-order or mean field type approximations. The inclusion of scattering effects is crucial and the leading-order approximation is approximately valid only for $t \ll 1/\gamma^{(\text{damp})}$.

reflection invariance and conservation of energy is preserved at each order in the $1/N$ expansion. For a discussion of similar approximation schemes applied to an N -component quantum anharmonic oscillator see also Ref. [22]. For $N=1$ the current approximation includes the type of diagrams involved in the three-loop approximation of the $2PI$ effective action used in Refs. [12, 13]. The precise correspondence can be found by neglecting all contributions of the current approximation beyond three-loop and rescaling the four-point function “ $L \rightarrow L/3$ ” in the three-loop approximation of Ref. [12].

We study the time evolution for two initial condition scenarios away from equilibrium. The first one corresponds to a “quench” (Sect. 7.1.1) often employed to mimic the situation of a rapidly expanding hot initial state which cools on time scales much smaller than the relaxation time of the fields [23]. Initially at high temperature we consider the relaxation processes following an instant “cooling” described by a sudden drop in the effective mass. The second scenario is characterized by initially densely populated modes in a

narrow momentum range around $\pm \mathbf{p}_{\text{ts}}$ (cf. Sect. 7.3.1). This initial condition has been termed “tsunami” in Ref. [24] and is reminiscent of colliding wave packets moving with opposite and equal momentum. A similar nonthermal and radially symmetric distribution of highly populated modes may also be encountered in a “color glass condensate” at saturated gluon density with typical momentum scale p_{ts} [25, 26]. Of course, a sudden change in the two-point function of a previously equilibrated system or a peaked initial particle number distribution are general enough to exhibit characteristic properties of nonequilibrium dynamics for a large variety of physical situations.

To reduce the numerical “cost” of following the evolution to sufficiently large times we present results for the 1 + 1 dimensional quantum field theory with spatially homogeneous correlations. We stress that in 1 + 1 dimensions many realistic questions can not be addressed, in particular since there is no spontaneous symmetry breaking. The 1 + 1 dimensional dynamics may help to understand the symmetric regime relevant for sufficiently high energy densities. However, the current results should be understood as a first controlled, quantitative approach to understand the dynamics of quantum fields far away from equilibrium.

Independent of the details of the initial conditions we find the following characteristic time scales summarized in Fig. 1. The nontrivial two- and four-point functions at next-to-leading order in $1/N$ oscillate with initial frequency proportional to the renormalized initial mass M_{INIT} . All correlation functions quickly approach an exponentially damped behavior. A characteristic rate $\gamma_0^{(\text{damp})}$ can be obtained from the zero mode of the unequal-time two-point function $F(t, 0; p = 0) = \langle \phi(t)\phi(0) \rangle_{p=0}$ with a corresponding time scale $\tau^{(\text{damp})}$ proportional to the inverse rate (Sect. 7.2). In this time range correlations with the initial state are effectively suppressed and asymptotically $F(t, 0; p = 0) \rightarrow 0^+$.

Both for the “quench” and the “tsunami” we observe that after the characteristic damping time the system is still far away from equilibrium. We find very different rates for damping and for the late-time exponential approach to thermal equilibrium³, i.e. $\tau^{(\text{damp})} \ll \tau^{(\text{therm})}$. Though the exponential damping at early times is crucial for an effective loss of details of the initial conditions — a prerequisite for the approach to equilibrium — it does not determine the time scale for thermalization. At intermediate

³For the employed spatially homogeneous initial conditions we do not observe a power-law “tail” for the late-time evolution (see also Ref. [27]).

times the evolution of correlation functions is found to be characterized by a parametrically slow change (drifting) for times typically much smaller than $\tau^{(\text{therm})}$. We observe characteristic power law behavior $|F(t, t; p) - F(0, 0; p)| \sim t^{(\text{power})_p}$ reminiscent of a hydrodynamic regime (Sect. 7.3). The large-time limit of correlation functions is determined by the (conserved) energy density and independent of the detailed initial conditions.

Apart from the three qualitatively different time regimes, whose presence is rather insensitive to the details of the initial conditions, there are nonequilibrium phenomena specific to a “quench” or a “tsunami” (cf. Sect. 7). After quenching from an initial thermal distribution with temperature T_0 we find that the system relaxes asymptotically to an effective particle number distribution with temperature (inverse slope parameter) $T < T_0$. During the nonequilibrium evolution the nontrivial two- and four-point correlation modes show no substantially different behavior for low or for high momenta in absence of spontaneous symmetry breaking. In contrast, the “tsunami” initial condition can lead to strong differences in the dynamics for the low ($p \ll p_{\text{ts}}$) and the high lying modes ($p \gg p_{\text{ts}}$). In particular, for the low momentum modes the inverse slope parameter quickly shoots up in response to the “tsunami” and can reach several T_{EQ} at intermediate times. The high momentum modes show the opposite effect and “cool” down slightly, before the inverse slope $T(x^0; p)$ approaches its asymptotic constant value T_{EQ} (cf. Sect. 7.4.1).

New phenomena of far-from-equilibrium physics include also the possible appearance of strongly interacting low momentum modes at intermediate times. For the employed “tsunami” of Sect. 7.3.1 the effective four-point function $\lambda_{\text{eff}}(x^0; p = 0)/6N$ reaches several times its initial value before it relaxes to its asymptotic late-time result, which is smaller than the initial value $\lambda/6N$ (cf. Sect. 7.3.3). The strong renormalization of the effective four-point function at intermediate times also stresses the fact that effective descriptions based on a clear separation of scales can be difficult to achieve for far-from-equilibrium processes.

Sects. 2 and 3 present a short introduction to the generating functional for nonequilibrium $2PI$ Green’s functions. In Sects. 4 and 5 we compute the $2PI$ effective action to next-to-leading order in $1/N$ and derive the equations of motion. Sect. 6 discusses the numerical implementation. The numerical results are given in Sect. 7, where we also present a comparison with leading-order results and determine the range of validity of mean field type approximations. We end with a conclusion and an outlook in Sect. 8.

2 $2PI$ effective action

We consider a quantum field theory with classical action $S = \int d^{d+1}x \mathcal{L}$,

$$\mathcal{L}(x; \varphi) = \frac{1}{2} \partial_{x^0} \varphi_a \partial_{x^0} \varphi_a - \frac{1}{2} \partial_{\mathbf{x}} \varphi_a \partial_{\mathbf{x}} \varphi_a - \frac{1}{2} m^2 \varphi_a \varphi_a - \frac{\lambda}{4!N} (\varphi_a \varphi_a)^2 \quad (2.1)$$

where $\varphi_a(x)$, $x \equiv (x^0, \mathbf{x})$, is a real, scalar field with $a = 1, \dots, N$ components (summation over repeated indices is implied). All correlation functions of the quantum theory can be obtained from the effective action $\Gamma[\phi, G]$, i.e. the generating functional for two-particle irreducible ($2PI$) Green's functions parametrized by the field $G_{ab}(x, y)$ representing an expectation value of the time ordered composite $T\varphi_a(x)\varphi_b(y)$ and the macroscopic field $\phi_a(x)$ given by the expectation value of $\varphi_a(x)$. A discussion of the defining functional integral of the $2PI$ effective action can be found in Ref. [8]. Following [8] it is convenient to parametrize the $2PI$ effective action as

$$\Gamma[\phi, G] = S[\phi] + \frac{i}{2} \text{Tr} \ln G^{-1} + \frac{i}{2} \text{Tr} G_0^{-1} G + \Gamma_2[\phi, G] + \text{const} \quad (2.2)$$

which expresses Γ in terms of the classical action S and correction terms including the function Γ_2 which is discussed below. Here the classical inverse propagator $iG_{0,ab}^{-1}(x, y; \phi) = \delta^2 S[\phi] / \delta\phi_a(x) \delta\phi_b(y)$ is given by

$$\begin{aligned} iG_{0,ab}^{-1}(x, y; \phi) &= - \left(\square_x + m^2 + \frac{\lambda}{6N} \phi_c(x) \phi_c(x) \right) \delta_{ab} \delta^{d+1}(x - y) \\ &\quad - \frac{\lambda}{3N} \phi_a(x) \phi_b(x) \delta^{d+1}(x - y). \end{aligned} \quad (2.3)$$

In absence of external sources physical solutions require

$$\frac{\delta\Gamma[\phi, G]}{\delta\phi_a(x)} = 0, \quad (2.4)$$

$$\frac{\delta\Gamma[\phi, G]}{\delta G_{ab}(x, y)} = 0. \quad (2.5)$$

Taking the derivative of (2.2) with respect to G one observes that the second stationarity condition (2.5) is equivalent to the exact Schwinger-Dyson equation for the propagator:

$$G_{ab}^{-1}(x, y) = G_{0,ab}^{-1}(x, y; \phi) - \Sigma_{ab}(x, y; \phi, G) \quad (2.6)$$

with the proper self energy

$$\Sigma_{ab}(x, y; \phi, G) = 2i \frac{\delta\Gamma_2[\phi, G]}{\delta G_{ab}(x, y)}. \quad (2.7)$$

The simple relation between the self energy and the correction term Γ_2 motivates the representation (2.2) of the $2PI$ effective action. It is instructive to observe from (2.7) that Γ_2 must be two-particle irreducible (cf. also the detailed discussion in Ref. [8]). For (2.6) to be an identity Σ is to be interpreted as the proper self energy where only one-particle irreducible graphs can contribute. Suppose Γ_2 has a two-particle reducible contribution of the form $\tilde{\Gamma}G\tilde{\Gamma}'$. Then Σ has a contribution of the form $\tilde{\Gamma}G\tilde{\Gamma}'$ since it is given by a derivative of Γ_2 with respect to G . Such a structure cannot occur for the proper self energy and two-particle reducible contributions to Γ_2 must be absent.

Truncated Schwinger–Dyson equations are often used to describe nonperturbative physics. Typically the employed approximation is based on some ansatz for Σ which in turn corresponds to an efficient resummation of a large number of graphs. It is apparent from the simple relation (2.7) that the $2PI$ effective action may be used as a powerful tool to obtain resummation schemes in a systematic way.

The contribution Γ_2 in (2.2) is given by all $2PI$ graphs with the propagator lines set equal to G [8]. (A graph is two-particle irreducible if it does not become disconnected upon opening two propagator lines.) In presence of a nonvanishing expectation value ϕ the $2PI$ graphs are constructed from two kinds of vertices described by the effective interaction Lagrangian

$$\mathcal{L}_{\text{INT}}(x; \phi, \varphi) = -\frac{\lambda}{6N}\phi_a(x)\varphi_a(x)\varphi_b(x)\varphi_b(x) - \frac{\lambda}{4!N}\left(\varphi_a(x)\varphi_a(x)\right)^2. \quad (2.8)$$

The effective interaction can be obtained from (2.1) by shifting the field $\varphi \rightarrow \varphi + \phi$. The terms cubic and higher in φ define the vertices from which the $2PI$ graphs contributing to Γ_2 can be constructed.

The relation of the $2PI$ effective action to the conventional generating functional for *one*-particle irreducible Green's functions is very simple. The $1PI$ effective action corresponds to $\Gamma[\phi, G]$ at that value of G for which (2.5) holds, i.e.

$$\Gamma[\phi] = \Gamma[\phi, G_{\text{stat}}] \quad , \quad \left. \frac{\delta\Gamma[\phi, G]}{\delta G(x, y)} \right|_{G=G_{\text{stat}}} = 0. \quad (2.9)$$

3 Nonequilibrium Green's functions

We will use the $2PI$ effective action to study the time evolution of n -point functions for given initial correlations at time t_I . The initial n -point functions $\text{Tr}\{\bar{\rho}(t_I)\varphi(t_I, \mathbf{x}_1)\dots\varphi(t_I, \mathbf{x}_n)\}$ may include a mixed-state density matrix $\bar{\rho}(t_I)$ for which $\text{Tr}\{\bar{\rho}^2(t_I)\} < 1$. This is necessary to allow for general nonequilibrium initial conditions and, in particular, if the initial density matrix describes thermal equilibrium. Often the initial conditions of an experiment — one may think of a scattering experiment of particles at an initial time t_I far before they reach the interaction region — may be described by only a few lowest n -point functions. For a setup which can be described in terms of an initial Gaussian density matrix the nonvanishing initial correlations are completely specified by ϕ and G and their first order time derivatives⁴ at t_I , i.e.

$$\begin{aligned}\phi(t_I, \mathbf{x}) &= \text{Tr}\{\bar{\rho}(t_I)\varphi(t_I, \mathbf{x})\}, \\ \dot{\phi}(t_I, \mathbf{x}) &= \text{Tr}\{\bar{\rho}(t_I)\partial_{x^0}\varphi(x^0, \mathbf{x})\}|_{x^0=t_I},\end{aligned}\tag{3.1}$$

and the initial two-point functions

$$\begin{aligned}G(t_I, \mathbf{x}; t_I, \mathbf{y}) &= \text{Tr}\{\bar{\rho}(t_I)\varphi(t_I, \mathbf{x})\varphi(t_I, \mathbf{y})\} - \phi(t_I, \mathbf{x})\phi(t_I, \mathbf{y}), \\ H(t_I, \mathbf{x}; t_I, \mathbf{y}) &= \text{Tr}\{\bar{\rho}(t_I)\partial_{x^0}\varphi(x^0, \mathbf{x})\varphi(t_I, \mathbf{y})\}|_{x^0=t_I} - \dot{\phi}(t_I, \mathbf{x})\phi(t_I, \mathbf{y}), \\ K(t_I, \mathbf{x}; t_I, \mathbf{y}) &= \text{Tr}\{\bar{\rho}(t_I)\partial_{x^0}\varphi(x^0, \mathbf{x})\partial_{y^0}\varphi(y^0, \mathbf{y})\}|_{x^0=y^0=t_I} - \dot{\phi}(t_I, \mathbf{x})\dot{\phi}(t_I, \mathbf{y}).\end{aligned}\tag{3.2}$$

We will assume in the following that the initial conditions can be described in terms of a Gaussian density matrix. It should be stressed at this point that a specific initial condition only restricts the experimental setup and represents no approximation for the time evolution. For $t > t_I$ irreducible higher n -point functions are induced by the time evolution of the interacting theory. The full $2PI$ effective action $\Gamma[\phi, G]$ contains all possible information about n -point functions for given initial conditions.

A more general $\bar{\rho}(t_I)$ involves the specification of nonzero higher initial n -point functions than (3.1) and (3.2). The $2PI$ effective action in presence

⁴ For a Gaussian initial mixed-state density matrix there are three independent variances which can be chosen as G , H and K defined in (3.2). Note that the initial correlation $\text{Tr}\{\bar{\rho}(t_I)\varphi(t_I, \mathbf{x})\partial_{y^0}\varphi(y^0, \mathbf{y})\}|_{y^0=t_I}$ is not independent because of the commutation relation between φ and $\partial_{y^0}\varphi$. A detailed discussion of Gaussian initial conditions can be found in Ref. [28].

of a more general initial density matrix is discussed in [10, 12]. In general, a non-Gaussian $\bar{\rho}(t_I)$ leads to additional source terms in the generating functional for $2PI$ Green's functions and Γ is no longer of the simple form (2.2). These source terms are non-vanishing at time t_I only and allow for the specification of the additional nonzero initial correlations.

For Gaussian initial conditions the time evolution of n -point functions $\text{Tr}\{\bar{\rho}(t_I)\varphi(x)\dots\varphi(y)\}$ is completely specified by (3.1) and (3.2) and known $\Gamma[\phi, G]$. It should be noted that the n -point functions of the initial time problem differ from those used to compute S -matrix elements in conventional scattering theory. The n -point functions for the initial time problem involve the trace over products of field operators. Stated differently, one computes matrix elements between same states. These are sometimes called “*in – in*” matrix elements in contrast to “*in – out*” matrix elements used in conventional scattering theory. The construction of the generating functionals for the respective n -point functions is identical up to the time path. The trace over products of field operators implies that the generating functional used for initial time problems involves a closed time path \mathcal{C} [1]. The time path starts at the initial time t_I and runs along the (real) time axis to some final time t and back to t_I . The largest time of the path t is kept as a parameter and is evolved in the time evolution equations for the fields as described in Sect. 5.2.⁵

4 $1/N$ expansion of the $2PI$ effective action

In the interacting theory the $2PI$ effective action cannot be computed exactly. In this work we employ a $1/N$ expansion of the $2PI$ effective action $\Gamma[\phi, G]$ where N is the number of field components. The leading order approximation is found by considering only those $2PI$ diagrams where the summation over internal lines yields a factor greater than or equal to N^l with l the number of loops in the diagram. The next-to-leading order diagrams yield a factor N^{l-1} , next-to-next-to-leading order N^{l-2} and so forth. This defines a systematic classification in terms of powers of $1/N$ for $2PI$ diagrams

⁵ Formulations of closed time path generating functionals often exhibit an infinite time interval $]-\infty, \infty[$. In this case the number of field labels has to be doubled to distinguish the fields on the underlying closed contour. Causality implies that for any n -point function at finite times t_i ($i = 1, \dots, n$) the contributions of the infinite time path employed in these formulations cancel for times larger than $\max(t_i)$. For our purposes of a possible numerical implementation as an initial-value problem the infinite time path is not useful.

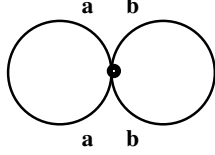


Figure 2: *LO* contribution to the *2PI* effective action.

contributing to $\Gamma[\phi, G]$. For a discussion of similar approximation schemes applied to quantum mechanics see also Ref. [22]. In the large- N limit ϕ_a can be taken to be $\mathcal{O}(\sqrt{N})$, hence G_{ab} is $\mathcal{O}(1)$ [8]. The leading order term is then proportional to N and the next-to-leading order term is proportional to one, as will be considered in the following.

4.1 *2PI* effective action to next-to-leading order

For simplicity we will concentrate in the following on the symmetric regime where it is sufficient to consider $\Gamma[\phi = 0, G] \equiv \Gamma[G]$. We write

$$\Gamma_2[G] = \Gamma_2^{\text{LO}}[G] + \Gamma_2^{\text{NLO}}[G] + \dots \quad (4.1)$$

where Γ_2^{LO} denotes the leading order (LO) and Γ_2^{NLO} the next-to-leading order (NLO) contributions. The dots indicate terms beyond the NLO approximation. The LO contribution to $\Gamma_2[G]$ is given by only one diagram shown in Fig. 2,

$$\Gamma_2^{\text{LO}}[G] = -\frac{\lambda}{4!N} \int_{\mathcal{C}} d^{d+1}x G_{aa}(x, x)G_{bb}(x, x). \quad (4.2)$$

Omitting combinatorial factors Fig. 3 indicates the diagrams contributing to $\Gamma_2[G]$ in next-to-leading order. The first diagram of the series corresponds to the double bubble diagram shown in Fig. 4. It is followed by a three-loop diagram shown and then each subsequent diagram of the NLO series can be constructed from the preceding one by introducing at one vertex an

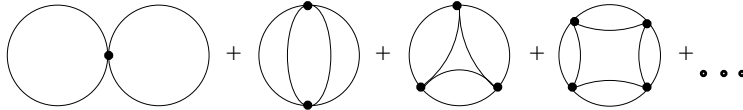


Figure 3: *NLO* contribution to the *2PI* effective action.

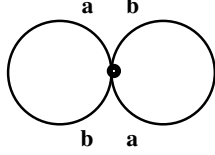


Figure 4: NLO “double bubble” contribution.

additional loop as in Fig. 3. One may view these contributions as a three-loop diagram with an effective four-vertex containing a “chain” of bubbles. The double bubble and the infinite series of closed chain diagrams are the only graphs contributing to $\Gamma_2[G]$ to NLO. For instance, the other $2PI$ five-loop diagram shown in Fig. 5 only contributes to NNLO. It is straightforward to sum the infinite number of NLO diagrams analytically. One finds

$$\Gamma_2^{\text{NLO}}[G] = \frac{i}{2} \int_{\mathcal{C}} d^{d+1}x \ln[\mathbf{B}(G)](x, x) \quad (4.3)$$

where

$$\mathbf{B}(x, y; G) = \delta_{\mathcal{C}}^{d+1}(x - y) + i \frac{\lambda}{6N} G_{ab}(x, y) G_{ab}(x, y). \quad (4.4)$$

It is instructive to expand the RHS of (4.3) to see the correspondence with the series of graphs in Fig. 3

$$\begin{aligned} \int_{\mathcal{C}} d^{d+1}x \ln[\mathbf{B}(G)](x, x) &= \int_{\mathcal{C}} d^{d+1}x \left(i \frac{\lambda}{6N} G_{ab}(x, x) G_{ab}(x, x) \right) \\ &\quad - \frac{1}{2} \int_{\mathcal{C}} d^{d+1}x d^{d+1}y \left(i \frac{\lambda}{6N} G_{ab}(x, y) G_{ab}(x, y) \right) \left(i \frac{\lambda}{6N} G_{a'b'}(y, x) G_{a'b'}(y, x) \right) \\ &\quad + \dots \end{aligned} \quad (4.5)$$

The contributions (4.2) and (4.3) constitute the NLO approximation for $\Gamma[G]$. We will use this without further approximations to derive the time evolution equation for G in Sect. 5, which parametrizes the generating

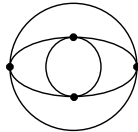


Figure 5: The five-loop $2PI$ “eye”-diagram contributes at $NNLO$.

functional $\Gamma[G]$. Once G is known for all times of interest the theory is “solved” in the symmetric regime to NLO: All correlation functions can be obtained from derivatives of the generating functional (2.2) and are given by (summed) diagrammatic expressions in terms of G .

4.2 Comparison with conventional $1/N$ schemes

We stress that in the above $2PI$ scheme the counting of orders of $1/N$ is done for diagrams with propagator lines associated to the field G . The time evolution for the propagator field is governed by a differential equation in G which is explicit in time and can be solved by standard techniques for given initial conditions (cf. Sect. 5.2). If not for a perturbative approximation there is no need to express G in terms of the classical propagator G_0 . However, to compare with standard $1/N$ expansions for the $1PI$ effective action G can be written as an infinite series parametrized by G_0 .

To leading order there is no difference to the conventional $1/N$ expansion scheme [8]. The equivalence can be observed using (2.7) and iteratively expanding the result for the full propagator (2.6) in powers of the coupling λ . This yields the solution of G in terms of an infinite series of diagrams with propagator lines associated to the classical propagator G_0 . Replacing this solution for G in (4.2) one recovers the conventional “bubble sum” expression for the leading order $1PI$ effective action.

Beyond leading order the counting for the $2PI$ effective action differs from the conventional $1/N$ expansion. The two schemes only differ by higher order terms. As an example, one may consider the three-loop diagram in Fig. 3. From (2.7) one finds that this diagram leads to the “setting sun” type contribution to the self energy shown in Fig. 6, where lines correspond to the full propagator G . Expressing the resulting G in terms of G_0 one observes, in particular, the resummation of an infinite series of “ladder” diagrams where two lines repeatedly exchange momenta by one-loop subdiagrams connecting the two lines. This infinite series of diagrams is not included in the conventional $1/N$ expansion at any finite order in $1/N$. A detailed discussion of the importance of these diagrams in the context of transport coefficients can be found in Refs. [2, 29].

In Sect. 7 we will observe that the employed approximation for the $2PI$ effective action leads to a bounded time evolution for the employed initial conditions, both at LO and NLO. In this case also the neglected term $\Gamma_2[G] - \Gamma_2^{\text{LO}}[G] - \Gamma_2^{\text{NLO}}[G]$ is finite at all times for a bounded full $\Gamma[G]$ or

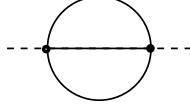


Figure 6: “Setting sun” type contribution to the self energy with lines G .

$\Gamma_2[G]$. The truncation error may therefore be controlled by its suppression with higher powers in $1/N$. This is in contrast to the conventional $1/N$ expansion for the $1PI$ effective action where terms grow unboundedly with time [7]. In the case of contributions which grow proportional to powers of t^a/N for some $a > 0$ such an expansion would break down at times of order $N^{1/a}$.

The $2PI$ effective action is known to lead to a non-secular time evolution already for the three-loop approximation of the $2PI$ effective action as has been pointed out in Ref. [12]. In Ref. [22] the N -component anharmonic oscillator, resumming an equivalent set of diagrams as discussed here, has also been shown to exhibit a bounded behavior. So far, we have not found initial conditions where this property could not be observed for the current approximation. To find the desirable analytical proof for arbitrary initial conditions is a difficult task in the presence of scattering and memory effects involved in the NLO time evolution, as is explained in the following.

5 Equation of motion

5.1 Schwinger–Dyson equation

According to (2.6) the exact inverse propagator can be written as

$$i G_{ab}^{-1}(x, y) = -(\square_x + m^2) \delta_{ab} \delta_C^{d+1}(x - y) - i \Sigma_{ab}(x, y; G) \quad (5.1)$$

where the full self energy Σ is given by (2.7). In next-to-leading order in $1/N$ the approximation for the self energy follows from the derivative of (4.2), (4.3) with respect to G_{ab} . One finds

$$\Sigma_{ab}(x, y; G) = -i \frac{\lambda}{6N} G_{cc}(x, x) \delta_{ab} \delta_C^{d+1}(x - y) - i \frac{\lambda}{3N} G_{ab}(x, y) \mathbf{B}^{-1}(x, y; G) \quad (5.2)$$

with \mathbf{B} given by (4.4). Multiplying (4.4) with \mathbf{B}^{-1} and using the identity $\int_C d^{d+1}z \mathbf{B}(x, z) \mathbf{B}^{-1}(z, y) = \delta_C^{d+1}(x - y)$ one observes that the inverse of \mathbf{B}

obeys

$$\mathbf{B}^{-1}(x, y; G) = \delta_{\mathcal{C}}^{d+1}(x - y) - i I(x, y). \quad (5.3)$$

Here the function $I(x, y)$ resums the “chain” of bubble graphs discussed in Sect. 4, i.e.

$$I(x, y) = \frac{\lambda}{6N} G_{ab}(x, y) G_{ab}(x, y) - i \frac{\lambda}{6N} \int_{\mathcal{C}} d^{d+1}z I(x, z) G_{ab}(z, y) G_{ab}(z, y). \quad (5.4)$$

Rewriting (5.3) and (5.4) we note that the combination

$$\frac{\lambda}{6N} \mathbf{B}^{-1}(x, y) = \frac{\lambda}{6N} \left(\delta_{\mathcal{C}}^{d+1}(x - y) - i \frac{\lambda}{6N} \int_{\mathcal{C}} d^{d+1}z \mathbf{B}^{-1}(x, z) G_{ab}(z, y) G_{ab}(z, y) \right) \quad (5.5)$$

plays the role of the (nonlocal) four-point function to order $1/N$.

In the symmetric regime we can evaluate (5.1) for the configuration $G_{ab}(x, y) = G(x, y) \delta_{ab}$. In this form the $\mathcal{O}(1)$ and $\mathcal{O}(1/N)$ contributions are explicit. We separate Σ in a local part and a nonlocal part,

$$\Sigma(x, y; G) = -i \Sigma^{(\text{local})}(x; G) \delta_{\mathcal{C}}^{d+1}(x - y) + \Sigma^{(\text{nonlocal})}(x, y; G). \quad (5.6)$$

Since $\Sigma^{(\text{local})}$ corresponds to a local mass shift it is convenient to write

$$M^2(x; G) = m^2 + \Sigma^{(\text{local})}(x; G). \quad (5.7)$$

With this notation the Schwinger–Dyson equation for the propagator reads

$$iG^{-1}(x, y) = -(\square_x + M^2(x; G)) \delta_{\mathcal{C}}^{d+1}(x - y) - i \Sigma^{(\text{nonlocal})}(x, y; G). \quad (5.8)$$

From (5.2)–(5.4) we observe that the local part receives LO and NLO contributions,

$$M^2(x; G) = m^2 + \lambda \frac{N+2}{6N} G(x, x), \quad (5.9)$$

while the inhomogeneous part of the self energy is nonvanishing only at NLO,

$$\Sigma^{(\text{nonlocal})}(x, y; G) = -\frac{\lambda}{3N} G(x, y) I(x, y), \quad (5.10)$$

where the resummed “chain” of bubble graphs (5.4) reads

$$I(x, y) = \frac{\lambda}{6} G(x, y) G(x, y) - i \frac{\lambda}{6} \int_{\mathcal{C}} d^{d+1}z I(x, z) G(z, y) G(z, y). \quad (5.11)$$

It is important to note that for the LO, or $N \rightarrow \infty$, approximation only a local mass shift is induced by the interactions. The NLO contribution is crucial in order to include direct scattering.

5.2 Initial-value time evolution

The form of the equation of motion (5.8) is suitable for a boundary value problem and can be used, in particular, to discuss the propagator in thermal equilibrium. However, nonequilibrium time evolution is an initial value problem. Here a suitable form of the equation of motion can be obtained by multiplying (5.8) by G from the right and by integration. With $\int_C d^{d+1}z G^{-1}(x, z)G(z, y) = \delta_C^{d+1}(x - y)$ one finds

$$(\square_x + M^2(x; G)) G(x, y) + i \int_C d^{d+1}z \Sigma^{(\text{nonlocal})}(x, z; G)G(z, y) = -i\delta_C^{d+1}(x - y) \quad (5.12)$$

This represents a second order differential equation for G which may be used to study the time evolution for given initial conditions (3.2). Very useful further simplification arises if we decompose

$$\begin{aligned} G(x, y) &= G_{>}(x, y)\Theta_C(x^0 - y^0) + G_{<}(x, y)\Theta_C(y^0 - x^0), \\ \Sigma^{(\text{nonlocal})}(x, y) &= \Sigma_{>}(x, y)\Theta_C(x^0 - y^0) + \Sigma_{<}(x, y)\Theta_C(y^0 - x^0) \end{aligned} \quad (5.13)$$

and observe

$$\square_x G(x, y) = \Theta_C(x^0 - y^0)\square_x G_{>}(x, y) + \Theta_C(y^0 - x^0)\square_x G_{<}(x, y) - i\delta_C^{d+1}(x - y). \quad (5.14)$$

Note that the equal-time commutation relation for the fields indeed imply

$$\frac{d}{dx^0} \left(G_{>}(x, y) - G_{<}(x, y) \right) \Big|_{x^0=y^0} = -i\delta^d(\mathbf{x} - \mathbf{y}). \quad (5.15)$$

For a real, scalar field theory $G_{>}^*(x, y) = G_{<}(x, y) = G_{>}(y, x)$ and all equations can be expressed in terms of one function ($G_{>}$) only. The self energy has the same properties $\Sigma_{>}^*(x, y) = \Sigma_{<}(x, y) = \Sigma_{>}(y, x)$, which can be verified from (5.10) and is valid to all orders in $1/N$. The Θ -functions in (5.14) are defined along the time contour C and can be evaluated

$$\begin{aligned} \int_C d^{d+1}z \Sigma^{(\text{nonlocal})}(x, z; G)G(z, y) &= \int d\mathbf{z} \left\{ \int_0^{y^0} dz^0 \Sigma_{>}(x, z; G)G_{>}(y, z) \right. \\ &\quad \left. + \int_{y^0}^{x^0} dz^0 \Sigma_{>}(x, z; G)G_{>}(z, y) - \int_0^{x^0} dz^0 \Sigma_{>}(z, x; G)G_{>}(z, y) \right\}. \end{aligned}$$

This yields the evolution equation

$$(\square_x + M^2(x; G)) G_{>}(x, y) = 2 \int d\mathbf{z} \left\{ \int_0^{x^0} dz^0 \text{Im} [\Sigma_{>}(x, z; G)] G_{>}(z, y) - \int_0^{y^0} dz^0 \Sigma_{>}(x, z; G) \text{Im} [G_{>}(z, y)] \right\}, \quad (5.16)$$

We note that (5.16) represents an exact equation for known local part $M^2(x; G)$ and nonlocal part $\Sigma_{>}(x, y; G)$ of the self energy (5.6).

5.3 Real-valued evolution equations

For the real scalar field theory there are two independent real-valued two-point functions, which can be associated to the expectation values of the commutator and the anti-commutator of two fields. We note that the field anti-commutator is determined by the real part and the commutator by the imaginary part of the complex function $G_{>}(x, y)$. Following Ref. [13] we define

$$F(x, y) = \frac{1}{2} \left(G_{>}(x, y) + G_{>}^*(x, y) \right) \equiv \text{Re}[G_{>}(x, y)], \quad (5.17)$$

$$\rho(x, y) = i \left(G_{>}(x, y) - G_{>}^*(x, y) \right) \equiv -2\text{Im}[G_{>}(x, y)] \quad (5.18)$$

where F is the “symmetric” propagator and ρ denotes the spectral function, with the property $F^*(x, y) = F(x, y) = F(y, x)$ and $\rho^*(x, y) = \rho(x, y) = -\rho(y, x)$. Similarly, we define

$$\Sigma_F(x, y) = \frac{1}{2} \left(\Sigma_{>}(x, y) + \Sigma_{>}^*(x, y) \right) \equiv \text{Re}[\Sigma_{>}(x, y)], \quad (5.19)$$

$$\Sigma_\rho(x, y) = i \left(\Sigma_{>}(x, y) - \Sigma_{>}^*(x, y) \right) \equiv -2\text{Im}[\Sigma_{>}(x, y)]. \quad (5.20)$$

The time evolution equations for F and ρ follow from (5.16) [13]

$$(\square_x + M^2(x; F)) F(x, y) = - \int d\mathbf{z} \left\{ \int_0^{x^0} dz^0 \Sigma_\rho(x, z; F, \rho) F(z, y) - \int_0^{y^0} dz^0 \Sigma_F(x, z; F, \rho) \rho(z, y) \right\}, \quad (5.21)$$

$$(\square_x + M^2(x; F)) \rho(x, y) = - \int d\mathbf{z} \int_{y^0}^{x^0} dz^0 \Sigma_\rho(x, z; F, \rho) \rho(z, y). \quad (5.22)$$

The form of the evolution equations for the symmetric propagator and the spectral function is independent of the approximation. They are equivalent to the exact Schwinger–Dyson equation (5.1), however, in the form (5.21) and (5.22) they are more suitable for initial time problems.

We note that due to the canonical commutation relations or (5.15) the spectral function obeys the equal-time properties

$$\rho(x, y)|_{x^0=y^0} = 0, \quad \partial_{x^0} \rho(x, y)|_{x^0=y^0} = \delta^d(\mathbf{x} - \mathbf{y}). \quad (5.23)$$

The time evolution of the spectral function is completely determined by (5.22) and (5.23).

In the NLO approximation $M^2(x; G)$ is given by (5.9), i.e.

$$M^2(x; F) = m^2 + \lambda \frac{N+2}{6N} F(x, x), \quad (5.24)$$

and from (5.10) and (5.11) one finds

$$\Sigma_F(x, y; F, \rho) = -\frac{\lambda}{3N} \left(F(x, y) I_F(x, y) - \frac{1}{4} \rho(x, y) I_\rho(x, y) \right), \quad (5.25)$$

$$\Sigma_\rho(x, y; F, \rho) = -\frac{\lambda}{3N} \left(F(x, y) I_\rho(x, y) + \rho(x, y) I_F(x, y) \right) \quad (5.26)$$

with⁶

$$\begin{aligned} I_F(x, y) &= \frac{\lambda}{6} \left(F^2(x, y) - \frac{1}{4} \rho^2(x, y) \right) \\ &- \frac{\lambda}{6} \int d\mathbf{z} \left\{ \int_0^{x^0} dz^0 I_\rho(x, z) \left(F^2(z, y) - \frac{1}{4} \rho^2(z, y) \right) \right. \\ &\quad \left. - 2 \int_0^{y^0} dz^0 I_F(x, z) F(z, y) \rho(z, y) \right\}, \end{aligned} \quad (5.27)$$

⁶Note that the resummed “chain” of bubbles (5.11) can be written as $I(x, y) = I_>(x, y) \Theta_C(x^0 - y^0) + I_<(x, y) \Theta_C(y^0 - x^0)$ with $I_>^*(x, y) = I_<(x, y) = I_>(y, x)$. With this notation $I_F(x, y) = \frac{1}{2}(I_>(x, y) + I_>^*(x, y)) = \text{Re}[I_>(x, y)]$ and $I_\rho(x, y) = i(I_>(x, y) - I_>^*(x, y)) = -2\text{Im}[I_>(x, y)]$.

$$\begin{aligned}
I_\rho(x, y) &= \frac{\lambda}{3} F(x, y) \rho(x, y) \\
&- \frac{\lambda}{3} \int d\mathbf{z} \int_{y^0}^{x^0} dz^0 I_\rho(x, z) F(z, y) \rho(z, y).
\end{aligned} \tag{5.28}$$

We emphasize that F , ρ , Σ_F and Σ_ρ are real functions, and one observes that the evolution equations (5.21)-(5.28) are causal and time-reversal invariant.

5.4 Comparison with thermal equilibrium

It is instructive to consider for a moment the quantities F and ρ , Σ_F and Σ_ρ , as well as I_F and I_ρ in thermal equilibrium. The $2PI$ effective action in thermal equilibrium, $\Gamma^{(\text{eq})}$, is given by the same expression (2.2), with (4.2) and (4.3) in the NLO large- N approximation, if the closed time path is replaced by an imaginary path $\mathcal{C} = [0, -i\beta]$. Here β denotes the inverse temperature. Since in equilibrium these functions depend only on the relative coordinates it is convenient to consider the Fourier transforms $F^{(\text{eq})}(\omega, \mathbf{p})$, $\rho^{(\text{eq})}(\omega, \mathbf{p})$, $\Sigma_F^{(\text{eq})}(\omega, \mathbf{p})$, $\Sigma_\rho^{(\text{eq})}(\omega, \mathbf{p})$, $I_F^{(\text{eq})}(\omega, \mathbf{p})$ and $I_\rho^{(\text{eq})}(\omega, \mathbf{p})$. From the periodicity (“KMS”) condition for the propagator in imaginary time, $G(x, y)|_{x^0=0} = G(x, y)|_{x^0=-i\beta}$, one infers the generic equilibrium relations⁷ (cf. also Ref. [13])

$$F^{(\text{eq})}(\omega, \mathbf{p}) = -i \left(n_B(\omega) + \frac{1}{2} \right) \rho^{(\text{eq})}(\omega, \mathbf{p}), \tag{5.29}$$

$$\Sigma_F^{(\text{eq})}(\omega, \mathbf{p}) = -i \left(n_B(\omega) + \frac{1}{2} \right) \Sigma_\rho^{(\text{eq})}(\omega, \mathbf{p}), \tag{5.30}$$

$$I_F^{(\text{eq})}(\omega, \mathbf{p}) = -i \left(n_B(\omega) + \frac{1}{2} \right) I_\rho^{(\text{eq})}(\omega, \mathbf{p}) \tag{5.31}$$

with $n_B(\omega) = (e^{\beta\omega} - 1)^{-1}$. Here we have used that with (5.11) and (5.10) the functions $I(x, y)$ and $\Sigma^{(\text{nonlocal})}(x, y)$ satisfy the same periodicity condition as $G(x, y)$.

While the spectral function $\rho^{(\text{eq})}$ encodes the information about the spectrum of the model, one observes that the symmetric function $F^{(\text{eq})}$ encodes the statistical aspects in terms of the particle distribution function n_B and similarly for the $\Sigma^{(\text{eq})}$ - and $I^{(\text{eq})}$ -functions. We note that the ratio

⁷In our conventions the Fourier transforms of the real-valued antisymmetric functions $\rho(x, y)$, $\Sigma_\rho(x, y)$ and $I_\rho(x, y)$ are purely imaginary.

$\Sigma_\rho^{(\text{eq})}(\omega, \mathbf{p})/2\omega$ plays in the limit of a vanishing ω -dependence the role of a decay rate for one-particle excited states with momentum \mathbf{p} . The function $I_\rho^{(\text{eq})}(\omega, \mathbf{p})$ encodes information about the effective vertex as will be discussed in Sect. 7.2.3. In the following we return to the nonequilibrium case and study the time evolution equations of Sect. 5.3.

6 Numerical implementation

The time evolution equations (5.21)–(5.28) are nonlinear, integro-differential equations. Though the equations are in general too complicated to be tackled analytically, they can be efficiently implemented and solved on a computer. Here it is important to note that all equations are explicit in time, i.e. all quantities at some later time t_f can be obtained by integration over the explicitly known functions for times $t < t_f$ with given initial conditions. This aspect is discussed in more detail below. In this respect, solving the initial time evolution equations for nonequilibrium problems is simpler than solving the corresponding gap equation of the form (5.8) self-consistently, which is typically employed for the study of thermal equilibrium. For simplicity we consider spatially homogeneous fields where

$$F(x, y) = F(x^0, y^0; \mathbf{x} - \mathbf{y}) = \int \frac{d\mathbf{p}}{(2\pi)^d} e^{i\mathbf{p}(\mathbf{x}-\mathbf{y})} F(x^0, y^0; \mathbf{p}) \quad (6.1)$$

and similarly for $\rho(x, y) = \rho(x^0, y^0; \mathbf{x} - \mathbf{y})$. Spatially inhomogeneous fields pose no additional complication but are computationally more expensive.

We employ a time discretization $x^0 = na_t$, $y^0 = ma_t$ with stepsize a_t , $F(x^0, y^0; \mathbf{p}) = F(n, m; \mathbf{p})$ and

$$\partial_{x^0}^2 F(x^0, y^0) \mapsto \frac{1}{a_t^2} \left(F(n+1, m) + F(n-1, m) - 2F(n, m) \right), \quad (6.2)$$

$$\int_0^{x^0} dt F(t, y^0) \mapsto a_t \left(F(0, m)/2 + \sum_{l=1}^{n-1} F(l, m) + F(n, m)/2 \right). \quad (6.3)$$

The above simple discretization leads already to stable numerics for small enough stepsize a_t (cf. also Refs. [12, 13]), but the convergence properties may be easily improved with more sophisticated standard estimators.

The discretized equations for the time evolution of the matrices $F(n, m)$ and $\rho(n, m)$ advance time stepwise in the “ n -direction” for fixed m . As for the

continuum the propagators obey the symmetry properties $F(n, m) = F(m, n)$ and $\rho(n, m) = -\rho(m, n)$. Consequently, only “half” of the (n, m) -matrices have to be computed and $\rho(n, n) \equiv 0$. Similarly, since I_ρ is antisymmetric in time $I_\rho(n, n)$ vanishes identically. It is also useful to note that $\rho(n+1, n) \equiv a_t$ is fixed by commutation relations (cf. Eq. (5.23)). As initial conditions one has to specify $F(0, 0; \mathbf{p})$, $F(1, 0; \mathbf{p})$ and $F(1, 1; \mathbf{p})$, while $\rho(0, 0; \mathbf{p}) = \rho(1, 1; \mathbf{p}) \equiv 0$ and $\rho(1, 0; \mathbf{p}) \equiv a_t$ are fixed.

The time discretized versions of the evolution equations (5.21) and (5.22),

$$\begin{aligned}
F(n+1, m; \mathbf{p}) &= 2F(n, m; \mathbf{p}) - F(n-1, m; \mathbf{p}) \\
&- a_t^2 \left\{ \mathbf{p}^2 + m^2 + \lambda \frac{N+2}{6N} \int \frac{d^d \mathbf{k}}{(2\pi)^d} F(n, n; \mathbf{k}) \right\} F(n, m; \mathbf{p}) \\
&- a_t^3 \left\{ \Sigma_\rho(n, 0; \mathbf{p}) F(0, m; \mathbf{p})/2 - \Sigma_F(n, 0; \mathbf{p}) \rho(0, m; \mathbf{p})/2 \right. \\
&\quad + \sum_{l=1}^{m-1} \left(\Sigma_\rho(n, l; \mathbf{p}) F(l, m; \mathbf{p}) - \Sigma_F(n, l; \mathbf{p}) \rho(l, m; \mathbf{p}) \right) \\
&\quad \left. + \sum_{l=m}^{n-1} \Sigma_\rho(n, l; \mathbf{p}) F(l, m; \mathbf{p}) \right\}, \tag{6.4}
\end{aligned}$$

$(n \geq m)$ ⁸ and similarly for ρ are explicit: Starting with $n = 1$, for the time step $n + 1$ one computes successively all entries with $m = 0, \dots, n + 1$ from known functions at earlier times. At first sight this property is less obvious for the non-derivative expressions (5.28) for I_F and (5.28) for I_ρ whose form is reminiscent of a gap equation. However, the discretized equation for I_ρ ,

$$\begin{aligned}
I_\rho(n, m; \mathbf{q}) &= \frac{\lambda}{3} \int \frac{d^d \mathbf{k}}{(2\pi)^d} \left\{ F(n, m; \mathbf{q} - \mathbf{k}) \rho(n, m; \mathbf{k}) \right. \\
&\quad \left. - a_t \sum_{l=m+1}^{n-1} I_\rho(n, l; \mathbf{q}) F(l, m; \mathbf{q} - \mathbf{k}) \rho(l, m; \mathbf{k}) \right\}, \tag{6.5}
\end{aligned}$$

shows that all expressions for $I_\rho(n, m)$ are explicit: Starting with $m = n$ where I_ρ vanishes one should lower $m = n, \dots, 0$ successively. For $m = n - 1$

⁸For the discretization of the time integrals it is useful to distinguish the cases $n \geq m$ and $n \leq m$. We compute the entries $F(n+1, m)$ from the discretized equations for $n \geq m$ except for $n+1 = m$ where we have to use the equations for $n \leq m$.

one obtains an explicit expression in terms of $F(n, m)$ and $\rho(n, m)$ known from the previous time step in n . For $m = n - 2$ the RHS then depends on the known function $I_\rho(n, n - 1)$ and so on. Similarly, for given $I_\rho(n, m)$ it is easy to convince oneself that the discretized Eq. (5.28) specifies $I_F(n, m)$ completely in terms of $I_F(n, 0), \dots, I_F(n, m - 1)$, which constitutes an explicit set of equations by increasing m successively.

It is crucial for an efficient numerical implementation that each step forward in time does not involve the solution of a self consistent or gap equation. This is manifest in the above discretization. The main numerical limitation of the approach is set by the time integrals (“memory integrals”) which grow with time and therefore slow down the numerical evaluation. Typically, the influence of early times on the late time behavior is suppressed and may be neglected numerically in a controlled way [30].

6.1 Continuum and infinite volume limit

We use a standard lattice discretization for a spatial volume V with periodic boundary conditions. For a spatial volume $V = (N_s a_s)^d$ with lattice spacing a_s and periodic boundary conditions momenta are given by

$$\mathbf{p}^2 \mapsto \sum_{i=1}^d \frac{4}{a_s^2} \sin^2 \left(\frac{a_s p_i}{2} \right), \quad p_i = \frac{2\pi n_i}{N_s a_s} \quad (6.6)$$

where $n_i = 0, \dots, N_s - 1$. The lattice introduces a momentum cutoff π/a_s . In order to obtain the theory in the continuum the lattice spacing has to be sent to zero and renormalization is necessary. In the following we consider numerical results in 1 + 1 dimensions. In this case the employed renormalization condition for the mass term, $M^2(x)|_{x^0=0} = M_{\text{INIT}}^2$, as described by (5.24) is sufficient to obtain finite, physical results.

In order to study the infinite volume limit one has to remove finite size effects. Here this is done by increasing the volume until convergence of the results is observed. Fig. 7 shows a typical time evolution of the unequal-time correlation zero mode $F(x^0, 0; p = 0)$ for three different volumes $L_* = N_s a_s = 256 \times 0.4/M_{\text{INIT}}$, $L_*/4$ and $L_*/16$. The initial conditions are the same as for Fig. 10 described in detail below. One observes that the damping tends to be stronger for smaller volumes. We find that increasing the volume beyond L_* does not change the results such that one could distinguish the curves in the plot ($< 1\%$). Depending on the initial condition

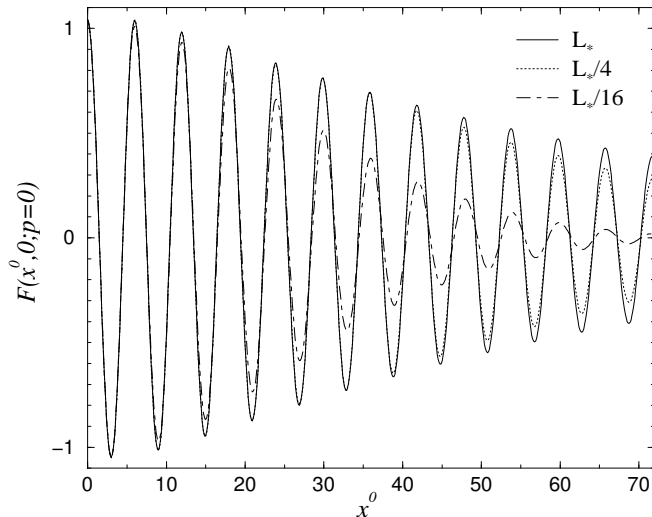


Figure 7: Volume dependence of the effective damping of oscillations, shown for the zero mode of the unequal-time function $F(x^0, 0; p)$ in the NLO approximation for three different volumes. Here $L_* = 256 \times 0.4/M_{\text{INIT}}$ denotes the “infinite” volume limit. The initial conditions are the same as for Fig. 10 and the evolution is discussed in detail below.

and the considered quantity the employed volumes can, however, be as large as $L = 1600 \times 0.4/M_{\text{INIT}}$ as for the LO evolution shown in Fig. 8, or as small as $L = 32 \times 0.2/M_{\text{INIT}}$ employed in the second frame of Fig. 13 showing the large-time behavior of the effective four-point function. (For the first frame of Fig. 13, showing the coupling at early times, we use $L = 256 \times 0.2/M_{\text{INIT}}$ and one observes a small volume dependence for the large-time behavior of this quantity.) We vary our lattice spacings in the range $a_s = (0.2 - 0.4)/M_{\text{INIT}}$ and $a_t/a_s = 0.05 - 0.2$.⁹

⁹ For time evolution problems the volume which is necessary to reach the infinite volume limit to a given accuracy can depend on the time scale. This is, in particular, due to the fact that finite systems can show characteristic recurrence times after which an initial effective damping of oscillations can be reversed. The observed damping can be viewed as the result of a superposition of oscillatory functions with differing phases or frequencies. The recurrence time is given by the time after which the phase information contained in the initial oscillations is recovered. Then the damping starts again until twice the recurrence time is reached and so on. In 1+1 dimensions we explicitly verify that in the LO approximation ($N \rightarrow \infty$) the observed recurrence times for the equal-time correlation $F(x, x)$ scales with the volume $L = N_s a_s$ or the number of degrees of freedom to infinity. We emphasize that the phenomenon of complete recurrences, repeating the full

7 Nonequilibrium dynamics: damping, drifting and thermalization

The spatially homogeneous solution of (5.21) or (5.22) in the limit of a free field theory ($\lambda = 0$) describes modes which oscillate with frequency $\sqrt{\mathbf{p}^2 + m^2}/2\pi$ for unequal-time functions $F(x^0, 0; \mathbf{p})$ and $\rho(x^0, 0; \mathbf{p})$, unless they are not identically zero. Equal-time correlation modes $F(x^0, x^0; \mathbf{p})$ oscillate either with twice that frequency or they are constant in time¹⁰. The latter corresponds to solutions which are translationally invariant in time, i.e. $F(x^0, y^0; \mathbf{p}) = F(x^0 - y^0; \mathbf{p})$ and $\rho(x^0, y^0; \mathbf{p}) = \rho(x^0 - y^0; \mathbf{p})$.

Time translation invariant solutions play an important role for the dynamics of nonequilibrium field theory. In the presence of interactions we will observe below that for a large variety of initial conditions all modes approach time translation invariant solutions at asymptotically large times. This qualitative property of the asymptotic solution can be observed both for the LO and the NLO approximation. However, at LO the large-time behavior depends explicitly on the (conserved) initial particle number distribution and thermalization cannot be observed as is shown below. In contrast, in the NLO approximation scattering is taken into account and the nonequilibrium late time result turns out to be insensitive to the detailed initial conditions, approaching a thermal equilibrium distribution which is determined by the (conserved) initial energy density. Following Ref. [31] we will call in the following time translation invariant solutions of the evolution equations fixed point solutions.

We stress that during the nonequilibrium time evolution there is no loss of details about the initial conditions in any strict sense. The evolution equations are time reflection invariant and at any time the evolution can be reversed and the initial conditions recovered¹¹. In particular, starting away from a time translation invariant solution no fixed point solution can ever be reached during the nonequilibrium evolution (cf. also the discussion

initial oscillation pattern after some characteristic time, is not observed once scattering is taken into account. Periodic recurrences can occur with smaller amplitudes as time proceeds and are effectively suppressed in the large-time limit even for small systems. As a consequence, in the NLO approximation we find that convergence of results to a given accuracy can be obtained for sufficiently large, fixed volumes independently of the time.

¹⁰ Note that for equal times $\rho(x^0, x^0; \mathbf{p}) \equiv 0$ according to Eq. (5.23).

¹¹ In this paper we consider closed systems without coupling to an external heat bath or external fields, which could provide sources or sinks of energy.

in Sect.7.1.1). However, fixed point solutions can be approached arbitrarily closely for sufficiently large times as is discussed below.

In the following we present our numerical results and provide a detailed explanation of the summary in Sect. 1. To make contact with earlier work [4] we begin with a short discussion of the dynamics for the LO approximation which can be characterized by a fixed point solution [32]. The LO fixed point is unstable once scattering is taken into account and we present the comparison with the NLO approximation afterwards.

7.1 The LO fixed point

The LO contribution to the effective action (4.2) adds a time dependent mass shift to the free field evolution equation. The resulting effective mass term $M^2(x)$, given by (5.24) for $N \rightarrow \infty$, is the same for all Fourier modes and each mode propagates “collisionlessly”. The evolution equation (5.21) for $F(x, y)$ becomes nonlinear. However, it remains local in time since the “scattering” contributions on the RHS are absent in the LO approximation. In this case one observes that the evolution of F decouples from ρ . In LO the spectral function does not influence the time evolution of the symmetric propagator similar to the free field theory limit.

7.1.1 “Quench”

In Fig. 8 we plot the evolution of $M^2(x)$ in the LO approximation as a function of time x^0 . The time evolution follows a “quench” described by an instant drop in the effective mass term from $M_0^2 = 2M_{\text{INIT}}^2$ to M_{INIT}^2 . (Cf. the discussion in Sect. 1.) The initial equilibrium high temperature ($T_0 = 2M_{\text{INIT}}$) particle number distribution is $n_0(p) = 1/(\exp[\sqrt{p^2 + M_0^2}/T_0] - 1)$. The sudden change in the effective mass term drives the system out of equilibrium and one can study its relaxation. We present $M^2(x)$ for three different couplings $\lambda = \lambda_0 = 0.5 M_{\text{INIT}}^2$ (bottom), $10\lambda_0$ (middle) and $40\lambda_0$ (top). For the plot all quantities are given in units of appropriate powers of the initial time mass $M_{\text{INIT}} = M(x)|_{x^0=0}$. One observes that $M^2(x)$ shoots up from M_{INIT}^2 in response to the “quench”. The initial oscillations with frequency M_{INIT}/π are damped and at large times $M^2(x)$ approaches a constant M_{FP}^2 depending on n_0 and λ .

If a strictly time translation invariant solution were reached, with $F(x, x) = F(x - x)$, then the LO mass term would be a constant and

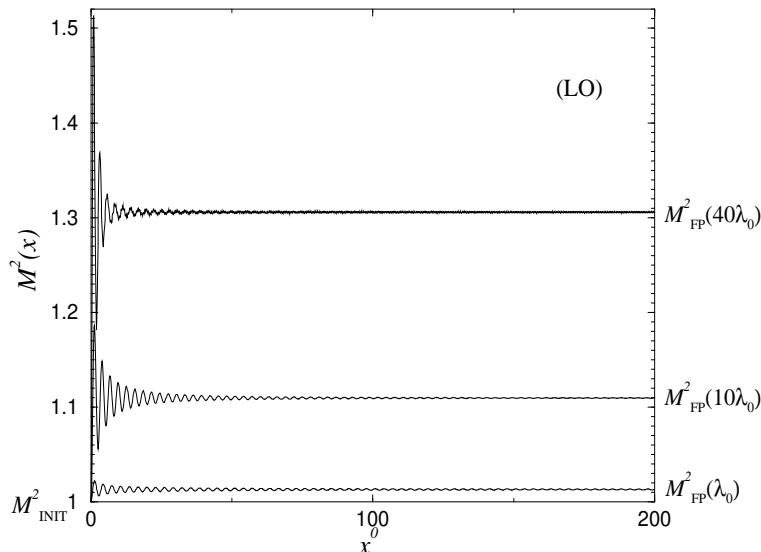


Figure 8: Shown is the mass term $M^2(x)$ in the LO approximation for three different couplings $\lambda = \lambda_0, 10\lambda_0, 40\lambda_0$ in units of appropriate powers of M_{INIT}^2 . The asymptotic constant M_{FP}^2 depends on the coupling and the initial particle number distribution n_0 . The value M_{FP}^2 is well described by the LO gap equation (7.1). The nonthermal LO fixed point becomes unstable once scattering is taken into account in the NLO approximation.

given by $M^2 = m^2 + \frac{\lambda}{6} F(x - x \equiv 0) = M_{\text{INIT}}^2$ according to Eq. (5.24) for $N \rightarrow \infty$. Clearly for the initial conditions employed in Fig. 8 the mass term is non-constant and the asymptotic values deviate from M_{INIT}^2 . We may compare the asymptotic dynamics with the solution of the LO equations for given particle number distribution $n_0(p)$ and an initial mass term such that $M^2(x) = M_{\text{GAP}}^2$ is constant. For a constant mass term the LO approximation behaves similar to a free theory. The propagator modes $F(x^0 - y^0; p) = [n_0(p) + 1/2] / \omega(p) \cos[\omega(p)(x^0 - y^0)]$ oscillate with $\omega = \sqrt{p^2 + M_{\text{GAP}}^2}$, where the effective mass term according to Eq. (5.24) is given by the LO gap equation¹²

$$M_{\text{GAP}}^2 = m^2 + \frac{\lambda}{6} \int \frac{dp}{2\pi} \left(n_0(p) + \frac{1}{2} \right) \frac{1}{\sqrt{p^2 + M_{\text{GAP}}^2}}. \quad (7.1)$$

¹² Here the logarithmic divergence of the one-dimensional integral is absorbed into the bare mass parameter m^2 using the same renormalization condition as for the dynamical evolution in the LO approximation, i.e. $m^2 + \frac{\lambda}{6} \int \frac{dp}{2\pi} (n_0(p) + \frac{1}{2}) (p^2 + M_0^2)^{-1/2} = M_{\text{INIT}}^2$.

The result from this gap equation is $M_{\text{GAP}}^2 = \{1.01, 1.10, 1.29\}M_{\text{INIT}}^2$ for the three values of λ . For this wide range of couplings the values are in good numerical agreement with the corresponding dynamical large time results inferred from Fig. 8 as $M_{\text{FP}}^2 = \{1.01, 1.11, 1.31\}M_{\text{INIT}}^2$ at $x^0 = 200/M_{\text{INIT}}$. We explicitly checked that at $x^0 = 400$ these values are still the same.

We stress that the particle number does not change during the LO time evolution and no approach to equilibrium is observed. Indeed the particle number

$$n(p) + \frac{1}{2} = \left(F(x^0, y^0; p) \partial_{x^0} \partial_{y^0} F(x^0, y^0; p) - (\partial_{x^0} F(x^0, y^0; p))^2 \right)^{\frac{1}{2}} \Big|_{x^0=y^0} \quad (7.2)$$

is a strictly conserved quantity in the LO approximation [28, 6, 32]. For the quench discussed above $\partial_{x^0} F(x^0, y^0; p)|_{x^0=y^0} \equiv 0$ with $n(p) = n_0(p)$ and the initial high temperature distribution remains constant.

We conclude that for the spatially homogeneous situation considered here the LO approximation cannot describe the approach to thermal equilibrium. The late time behavior is characterized by the LO fixed point which explicitly depends on the initial particle number distribution. This nonthermal fixed point becomes unstable once scattering is taken into account as is discussed in the following. Before we address the nonequilibrium dynamics in the NLO approximation in more detail we note from Eqs. (5.21) and (5.22) that the LO approximation for $F(x, y)$ and $\rho(x, y)$ becomes exact¹³ for $x^0, y^0 \rightarrow 0$. For very early times one therefore expects the LO approximation to yield a quantitatively valid description. This expectation is the basis for the many applications of the LO approximation found in the literature so far. Within the present framework we can test when the LO approximation breaks down by comparing it with the NLO results. We will see that the LO approximation fails to describe the main qualitative aspects of an early time exponential damping or late time approach to thermal equilibrium. However, for weak enough couplings certain time-averaged quantities at early times can be well determined by the LO fixed point solution. The particular role of the LO fixed point solution for time-averaged quantities at early times was pointed out for the classical field theory limit in Ref. [32].

¹³ This is due to the fact that we choose to consider Gaussian initial conditions, where at $x^0, y^0 = 0$ irreducible n -point functions vanish identically for $n > 2$.

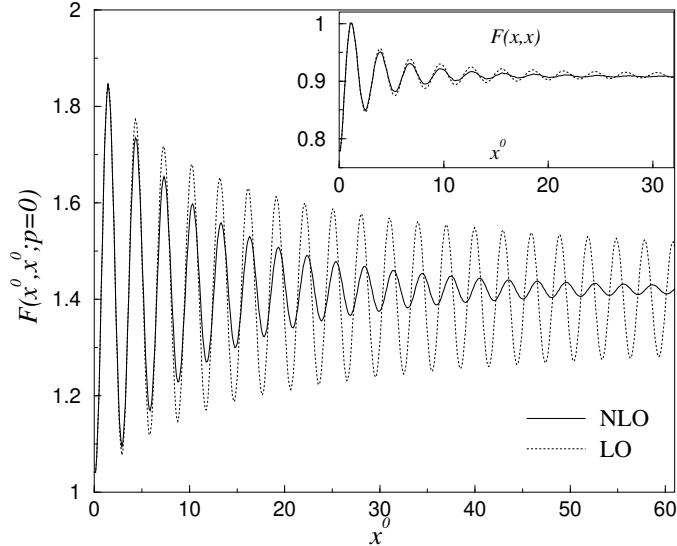


Figure 9: Time dependence of the equal-time zero mode $F(x^0, x^0; p = 0)$ after a “quench”. The employed coupling is $\lambda/6N = (5/6N \simeq 0.083) M_{\text{INIT}}^2$ for $N = 10$. The inset shows $F(x, x)$ which is the sum over all momentum modes. (All in units of appropriate powers of M_{INIT} .)

7.2 Early-time exponential damping

In contrast to the LO approximation at NLO in the $1/N$ expansion the evolution equations (5.21) and (5.22) include the nonlocal parts of the self energy, Σ_F and Σ_ρ , which encode scattering effects. In particular, the equations become nonlocal in time and the evolution depends on the time history. As pointed out above these memory effects can already be observed on the level of the exact equations (5.21) and (5.22) for known $\Sigma_{F,\rho}$. The time structure of the equations reflects causality and time reflection invariance which is preserved in the $1/N$ expansion scheme.

In Fig. 9 the solid line shows the behavior of the zero momentum mode of the equal-time correlator $F(x^0, x^0; p)$ in the NLO approximation after a “quench”. The inset displays the sum over all equal-time modes, $F(x, x) = \int \frac{dp}{2\pi} F(x^0, x^0; p)$, and $M^2(x)|_{x^0=0} = M_{\text{INIT}}^2$. The coupling is $\lambda/6N = (5/6N \simeq 0.083) M_{\text{INIT}}^2$ for $N = 10$ and the initial particle number distribution $n_0(q)$ is the same as described in Sect. 7.1 for the LO approximation. For comparison the dotted lines in Fig. 9 show the corresponding LO evolution.

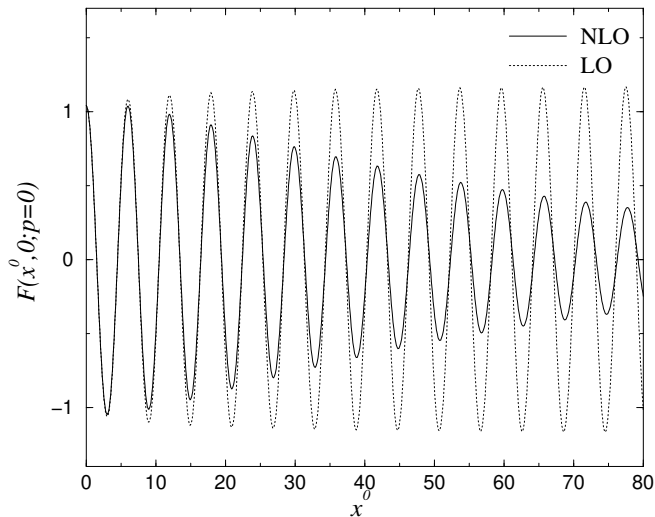


Figure 10: Shown is the evolution of the unequal-time correlation $F(x^0, 0; p = 0)$ after a “quench”. Unequal-time correlation functions approach zero in the NLO approximation and correlations with early times are effectively suppressed. (In units of $M_{\text{INIT.}}$)

7.2.1 Damping

As expected from the previous discussion, for very early times the NLO behavior is well described by the LO approximation. However, one observes that the damping of oscillations is more efficient at NLO due to scattering effects. The amplitude of the zero mode $F(x^0, x^0; p = 0)$ in Fig. 9 at NLO shows a substantial difference to the LO one. Summed over all momentum modes, however, the difference becomes less as can be inferred from $F(x, x)$ shown in the inset of the Figure. The different damping behavior becomes even more pronounced for unequal-time correlators. In Fig. 10 we plot $F(x^0, 0; p = 0)$ as a function of time. In sharp contrast to the NLO result, where the maximum amplitude of the correlation mode is damped, one observes that the LO correlator is not damped at all — in accordance with the LO fixed point behavior described in the previous section. We find that the unequal-time two-point functions approach zero in the NLO approximation and correlations with early times are therefore suppressed once scattering is taken into account. We stress that time-reversal invariance implies that the oscillations can never be damped out to zero completely during the nonequilibrium time evolution, however, zero can be approached arbitrarily

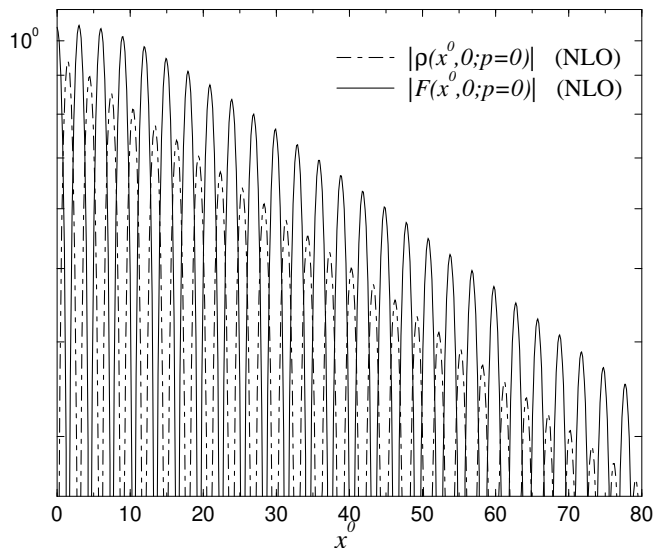


Figure 11: The correlation modes oscillations quickly approach an exponentially damped behavior. The logarithmic plot of $|\rho(x^0, 0; p = 0)|$ and $|F(x^0, 0; p = 0)|$ as a function of time x^0 shows an oscillation envelope approaching a straight line (in units of M_{INIT}).

closely.

In the NLO approximation we find that all modes $F(x^0, y^0; p)$ and $\rho(x^0, y^0; p)$ approach an approximately exponential damping behavior for both equal-time and unequal-time correlations. In Fig. 11 the approach to an exponential behavior is demonstrated for the unequal-time functions $|\rho(x^0, 0; p = 0)|$ and $|F(x^0, 0; p = 0)|$. The logarithmic plot shows that after a non-exponential period at very early times the envelope of oscillations can be well approximated by a straight line. From an asymptotic envelope fit of $F(x^0, 0; p = 0)$ to an exponential form $\sim \exp(-\gamma_0^{(\text{damp})} t)$ we obtain a damping rate $\gamma_0^{(\text{damp})} = 0.016 M_{\text{INIT}}$.

We conclude that, though strict dissipation can never be observed in a time-reversal invariant and energy conserving system, characteristic features of dissipative systems like exponential damping can be realized to very good approximation. The fact that correlation functions show an effective exponential damping once scattering is taken into account seems not to depend on the details of the approximation. We have observed the same qualitative feature in a three-loop expansion of the $2PI$ effective action [12, 13].

7.2.2 Effective mass

One observes from Fig. 9 that the correlation mode $F(x^0, x^0; p = 0)$ shoots up after the “quench” and relaxes. The initial oscillation frequency of the equal-time mode, M_{INIT}/π , changes only slowly. The early-time behavior of the NLO mass term $M^2(x)$ is rather well described by an oscillation around the LO fixed point value. The latter can be estimated from the solution of the LO gap equation (7.1), as described in Sect. 7.1, which yields $1.10M_{\text{INIT}}^2$. Comparing this with the average value for $M^2(x)$ for the time interval $0 < x^0 < 60/M_{\text{INIT}}$ we find a similar value $\overline{M}^2 = 1.13M_{\text{INIT}}^2$.

One may ask if the agreement can be further improved for not too late times by comparing it with an “improved” LO (Hartree) approximation, LO^+ , that takes into account the local part of the NLO self energy contribution (cf. Sect. 5.1). In this approximation one neglects the memory integrals on the RHS of the NLO evolution equations (5.21) and (5.22). The resulting equations are local in time and have the same structure as the LO ones, however, with the LO and NLO contribution to the mass term $M^2(x)$ included as given by Eq. (5.24). The large-time limit of the mass term in the LO^+ approximation is determined by the LO^+ fixed point solution in complete analogy to the discussion in Sect. 7.1. The fixed point value can be estimated from the corresponding gap equation which yields the asymptotic LO^+ value $1.11M_{\text{INIT}}^2$. The value slightly improves the LO result.

Figs. 9–11 gave an example for the nonequilibrium evolution after a “quench” for weak effective coupling where the damping rate is much smaller than the frequency of oscillations, i.e. $1 \gg \gamma_0^{(\text{damp})}/(\sqrt{M^2}/2\pi) = 0.09$ for the employed coupling $\lambda/6N = 0.083 M_{\text{INIT}}^2$. In the following we consider a “quench” with a larger drop in the effective mass term $M_0^2/M_{\text{INIT}}^2 = 2.91$ and a stronger effective coupling $\lambda/6N = 0.17 M_{\text{INIT}}^2$ for $N = 4$. The initial particle number distribution is $n_0(p) = 1/(\exp[\sqrt{p^2 + M_0^2}/T_0] - 1)$ with $T_0 = 8.47M_{\text{INIT}}$. As a consequence of the larger effective coupling the correlation functions exhibit stronger damping. The damping rate obtained from an exponential fit to the asymptotic behavior of $F(x^0, 0; p = 0)$ is found to be $\gamma_0^{(\text{damp})} = 0.11M_{\text{INIT}}$. We observe that the oscillation frequency of $F(x^0, 0; p = 0)$ quickly stabilizes around $1.10M_{\text{INIT}}/2\pi = 0.18M_{\text{INIT}}$ which is of the same order than the damping rate. Correspondingly, one finds from Fig. 12 an equal-time zero mode $F(x^0, x^0; p = 0)$ which is effectively damped out at NLO after a few oscillations. The deviation from the LO^+ result

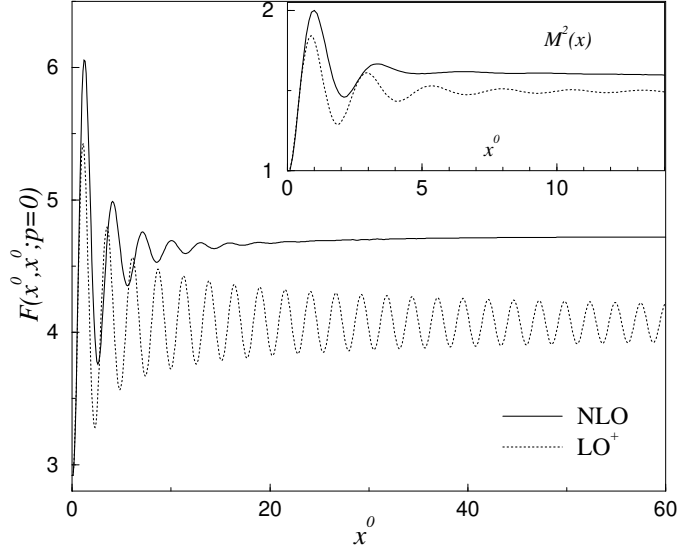


Figure 12: Time dependence of the equal-time zero mode $F(x^0, x^0; p = 0)$ after a “quench”, similar to Fig. 9 but not in the weak coupling regime (here $2\pi\gamma_0^{(\text{damp})}/\epsilon_0 \sim \mathcal{O}(1)$). The inset shows the mass term $M^2(x)$.

is substantial. From the inset of Fig. 12 one observes after a short initial period an almost constant mass term with a value $M^2(x) \simeq 1.6M_{\text{INIT}}^2$. The deviation of $M^2(x)$, which contains the sum over all equal-time modes, from the corresponding LO^+ value of about $1.5M_{\text{INIT}}^2$ is less severe than for the correlation modes.

We note that the relatively large value for $M^2(x)$ inferred from Fig. 12 does not characterize well the oscillation frequencies of the correlation zero modes. Following Ref. [13] a better characterization for the mode frequencies can be obtained from an effective mode energy defined as

$$\epsilon_p(x^0) \equiv \left(\frac{\partial_{x^0} \partial_{y^0} F(x^0, y^0; p)}{F(x^0, y^0; p)} \right)^{\frac{1}{2}} \Big|_{x^0=y^0} \quad (7.3)$$

which coincides with the dispersion relation of a free theory for $\lambda \rightarrow 0$. After a short oscillation period we find an almost constant value $\epsilon_0(x^0) \simeq 1.1M_{\text{INIT}}$. One observes that $\epsilon_0/2\pi$ is in good agreement with the oscillation frequency for $F(x^0, 0; p = 0)$ given above. A strongly damped behavior may therefore be characterized by

$$\frac{2\pi\gamma_0^{(\text{damp})}}{\epsilon_0} \gtrsim 1. \quad (7.4)$$

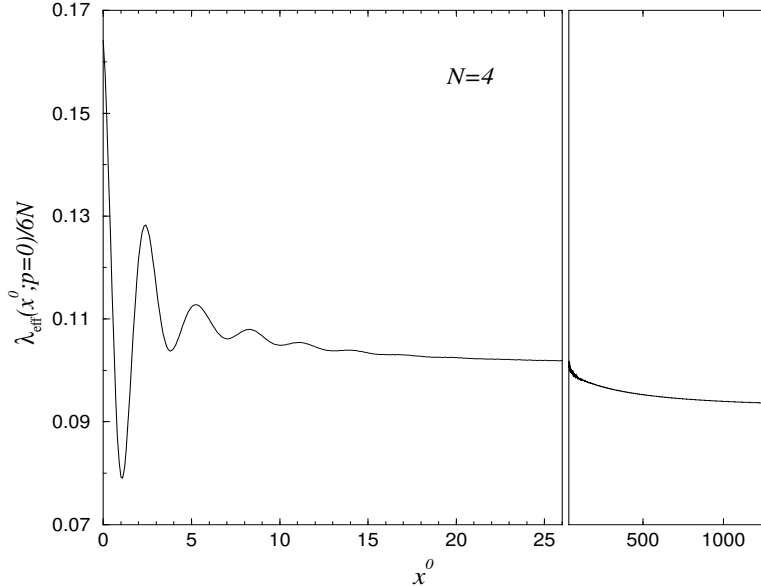


Figure 13: Nonequilibrium evolution of the effective four-point coupling at NLO for the initial conditions of Fig. 12 (in units of M_{INIT}). The added frame shows the large-time behavior for $x^0 > 26/M_{\text{INIT}}$ on a different scale.

7.2.3 Effective coupling

The nonlocal NLO four-point function (5.5) can be cast into an effective local coupling by integration over one variable. For spatially homogeneous initial conditions we define the time-dependent effective coupling

$$\begin{aligned}
 \frac{\lambda_{\text{eff}}}{6N}(x^0; p) &= \int_{\mathcal{C}} dy^0 \frac{\lambda}{6N} \mathbf{B}^{-1}(x^0, y^0; p) = \frac{\lambda}{6N} \left(1 - i \int_{\mathcal{C}} dy^0 I(x^0, y^0; p) \right) \\
 &= \frac{\lambda}{6N} \left(1 - \int_0^{x^0} d^{d+1}y I_{\rho}(x^0, y^0; p) \right). \tag{7.5}
 \end{aligned}$$

One observes that the effective coupling is determined by the antisymmetric function $I_{\rho}(x^0, y^0; p)$ given in Eq. (5.28).

The nonequilibrium evolution of $\lambda_{\text{eff}}/6N(x^0; p = 0)$ is shown in Fig. 13 for the same initial conditions as for Fig. 12. The effective coupling drops in response to the “quench” and after a short oscillatory period it exhibits a slowly changing behavior. We find a weak dependence of $\lambda_{\text{eff}}/6N(x^0; p)$ on momentum. We note that for the employed Gaussian initial conditions

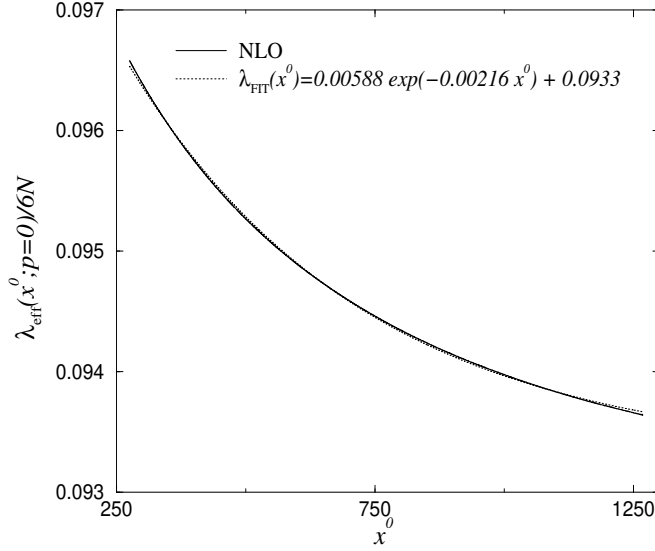


Figure 14: The same large-time behavior of the effective four-point coupling at NLO as in Fig. 13. Shown is a comparison with the exponential fit given in the Figure (all in units of M_{INIT}). One observes for $x^0 \gtrsim 250/M_{\text{INIT}}$ a very good approximation by an exponential with the small rate $\gamma_{\text{therm}} \simeq 2.2 \times 10^{-3} M_{\text{INIT}}$ for the approach to equilibrium (cf. Sect. 7.4).

the time evolution starts with the classical vertex $\sim \lambda$ parametrizing the action S , with no radiative or thermal corrections included. At large times, when the theory starts to thermalize, the four-point vertex approaches its renormalized equilibrium value as is discussed below¹⁴.

7.3 Non-exponential drifting at intermediate times

We emphasize that the characteristic time scale for damping $\tau^{(\text{damp})} \sim 1/\gamma_0^{(\text{damp})}$ does *not* correspond in general to the time scale for thermalization. Following a “quench” the initial rapid oscillations are effectively damped after $\tau^{(\text{damp})}$, however, the system is typically still far away from equilibrium. As an example, the right frame of Fig. 13 shows the asymptotic late-time behavior of the four-point function zero mode $\lambda_{\text{eff}}(x^0; p = 0)/6N$ for the

¹⁴ In this respect the time evolution is reminiscent of the Wilsonian renormalization group flow of couplings, where the flow interpolates between the classical or microscopic parameters and the macroscopic ones [33].

“quench” described above. Its asymptotic time dependence is very well approximated by an exponential behavior with rate $\gamma_{\text{therm}}^{(\lambda)} \simeq 2.2 \times 10^{-3} M_{\text{INIT}}$ as is demonstrated in Fig. 14 for a wide range of times. This rate characterizes the late-time approach to thermal equilibrium (cf. Sect. 7.4). It is much smaller than the damping rate and for the employed initial condition the corresponding time scales differ by almost two orders of magnitude.

We also note that the evolution of λ_{eff} in Fig. 13, after time-averaging over the oscillation time $\sim (\bar{\epsilon}_0)^{-1}$, cannot be approximated by a simple exponential before times of $\mathcal{O}(50/M_{\text{INIT}})$. The time dependence is parametrically much slower than an exponential and for $x^0 \gtrsim 1/\gamma_0^{(\text{damp})}$ better approximated by a power law behavior. Indeed, for a large variety of initial conditions we find a slow change or drifting of equal-time correlation modes over time scales τ_{drift} which are typically much larger than $\tau^{(\text{damp})}$. In the following we address the question in more detail of what happens at intermediate times $\tau^{(\text{damp})} \lesssim x^0 \lesssim \tau^{(\text{therm})}$, between the two time scales $\tau^{(\text{damp})}$ and $\tau^{(\text{therm})}$ which are both well characterized by an exponential rate.

7.3.1 “Tsunami”

More than for the above “quench”, the characteristic drifting time scale becomes apparent for a “tsunami” initial condition [24] (cf. Sect. 1). In the following we consider an initial particle number $n_0(p)$ distributed by a Gaussian

$$n_0(p) = \mathcal{A} \exp\left(-\frac{1}{2\sigma^2}(|p| - p_{\text{ts}})^2\right) \quad (7.6)$$

peaked around $|p| = p_{\text{ts}} = 5M_{\text{INIT}}$ with a width determined by $\sigma = 0.5M_{\text{INIT}}$ and amplitude $\mathcal{A} = 10$. The initial symmetric two-point function is $F(x^0, y^0; p)|_{x^0=y^0=0} = (n_0(p) + 1/2)/\sqrt{p^2 + M^2(0)}$ with $\partial_{x^0} F(x^0, y^0; p)|_{x^0=y^0=0} = 0$ and $F(x^0, y^0; p) \partial_{x^0} \partial_{y^0} F(x^0, y^0; p)|_{x^0=y^0=0} = [n_0(p) + 1/2]^2$. The distribution is symmetric under $p \rightarrow -p$ and reminiscent of two colliding wave packets in one spatial dimension. The units are given in terms of the renormalized initial *vacuum* mass (5.24) determined by $M_{\text{INIT}} = M(x)|_{x^0=0}$ for $n_0(p) \equiv 0$. Note that this is different from the initial effective mass $M(x)|_{x^0=0}$ for the nonvanishing particle distribution, $n_0(p) \neq 0$, as used above.

Similar to what is observed for the “quench” in Fig. 11, the unequal-time correlation modes $F(x^0; 0; p)$ and $\rho(x^0; 0; p)$ for the “tsunami” in the NLO approximation quickly approach an exponential damping behavior. Here the

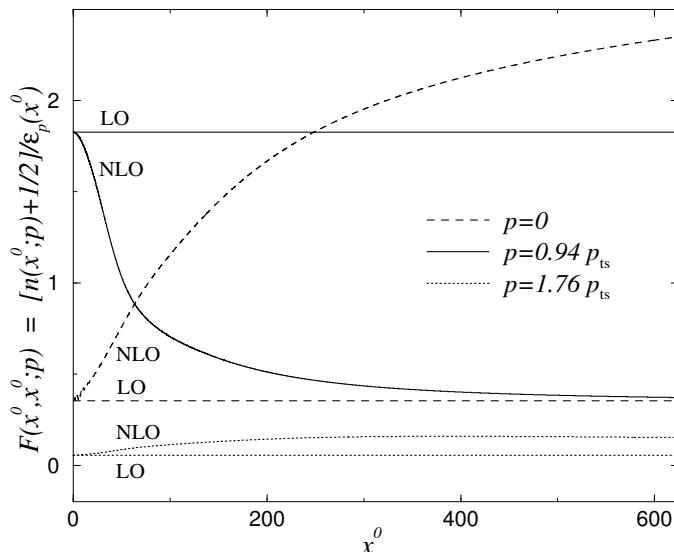


Figure 15: Comparison of the LO and NLO time dependence of the equal-time correlation modes $F(x^0, x^0; p)$ for the “tsunami” initial condition. The importance of scattering included in the NLO approximation is apparent: the correlation modes $F(x^0, x^0; p)$ drift away from the LO result and the “tsunami” decays, approaching thermal equilibrium at large times.

damping rate for the zero modes is $\gamma_0^{(\text{damp})} = 0.022M_{\text{INIT}}$. If we compare this with their oscillation frequency or ϵ_0 , as discussed below Eq. (7.3), one finds

$$2\pi\gamma_0^{(\text{damp})}/\epsilon_0 \simeq 0.01. \quad (7.7)$$

The considered “tsunami” is clearly in the weakly damped regime, which is due to a small effective coupling $\lambda/6N = 0.1M_{\text{INIT}}^2$ with $N = 10$.

In Fig. 15 we present the time evolution of the equal-time correlation modes $F(x^0, x^0; p)$ for different momenta. Shown are the LO and NLO results for zero momentum, close to the “tsunami” momentum p_{ts} and about twice p_{ts} . One observes that the LO equal-time correlations are constant in time. This behavior can be understood from the fact that for the employed “tsunami” initial condition the evolution starts at a time translation invariant fixed point solution of the LO equations described in Sect. 7.1.

Scattering effects included in the NLO approximation drive the system away from the LO fixed point. The equal-time correlation modes can be

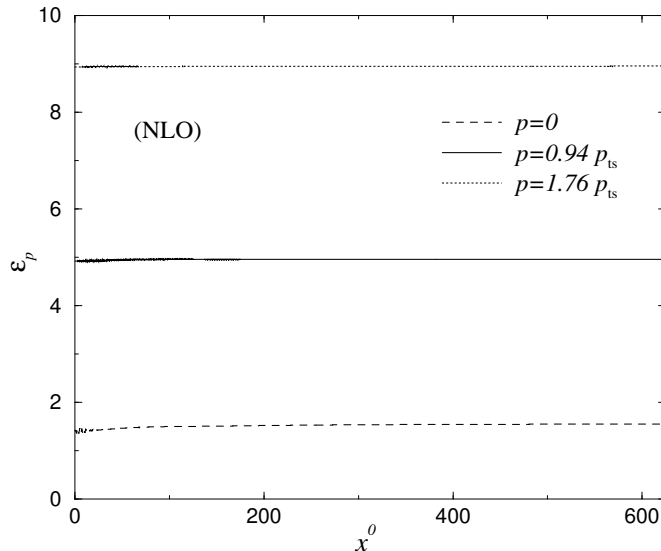


Figure 16: Effective mode energy $\epsilon_p(x^0)$, defined in Eq. (7.3), for the “tsunami” initial condition of Fig. 15. Comparison with the latter figure shows that despite substantial changes in the effective particle number the dispersion relation remains almost unchanged.

interpreted as the ratio of effective particle number¹⁵ [13]

$$n(x^0; p) + \frac{1}{2} \equiv \left(F(x^0, y^0; p) \partial_{x^0} \partial_{y^0} F(x^0, y^0; p) \right)^{\frac{1}{2}} \Big|_{x^0=y^0} \quad (7.8)$$

and effective mode energy $\epsilon_p(x^0)$ as defined in Eq. (7.3), i.e. $F(x^0, x^0; p) \equiv [n(x^0; p) + 1/2]/\epsilon_p(x^0)$. From Fig. 15 one observes that the zero momentum mode (dashed line) gets more and more populated as time proceeds, while the high momentum mode (dotted line) exhibits relatively small changes. The highly populated modes near $|p_{ts}|$ become less populated and the “tsunami” decays with time (solid line).

For comparison we show in Fig. 16 the time dependence of $\epsilon_p(x^0)$ for the corresponding momenta. As pointed out in Sect. 7.2.2 this quantity gives a good description for the oscillation frequencies of the two-point function modes. One observes from the figure that after a short oscillatory period and a small increase of $\epsilon_p(x^0)$ for low momenta, the effective mode energy is almost

¹⁵For time-translation invariant two-point functions this definition corresponds to (7.2) with $\partial_{x^0} F(x^0 - y^0; p)|_{x^0=y^0} \equiv 0$.

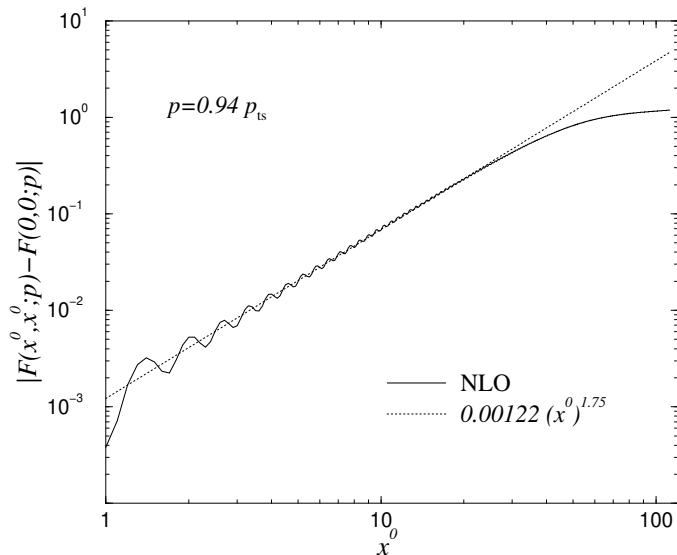


Figure 17: Double logarithmic plot for the equal-time mode $F(x^0, x^0; p)$ close to the “tsunami” momentum p_{ts} . The dotted straight line corresponds to a power law behavior $\sim (x^0 M_{\text{INIT}})^{1.75}$. The fit describes $F(x^0, x^0; p)$ very well for $x^0 \lesssim 30/M_{\text{INIT}}$ if time-averaged over the oscillation period. At later times the power law behavior changes to an exponential approach to thermal equilibrium.

constant in time. This is in sharp contrast to the substantial changes in the effective particle number as can be inferred from Fig. 15. A similar observation has been pointed out in Ref. [13] using the three-loop approximation.

7.3.2 Power law drifting

We point out that the decay of the “tsunami” modes is *not* governed by an exponential time dependence, here on a time scale $\tau^{(\text{drift})} \ll \tau^{(\text{therm})}$. The deviation of the equal-time correlation modes from the LO fixed point is rather well approximated by a power law behavior and thus parametrically slower than the exponential damping or late-time behavior. In particular, we find that the symmetric two-point function behaves approximately as

$$|F(x^0, x^0; p) - F(0, 0; p)| \sim (x^0)^{(\text{power})_p} \quad (7.9)$$

This is demonstrated in the double logarithmic plot of Fig. 17 for $F(x^0, x^0; p = 0.94 p_{\text{ts}})$. The NLO curve (solid line) oscillates around, and

quickly converges to, the (dotted) straight line fit characterizing a power law. Time-averaged over the oscillation period the evolution of the equal-time mode is well approximated by $\sim (x^0 M_{\text{INIT}})^{1.75}$ for $x^0 \lesssim 30/M_{\text{INIT}}$. The details of the intermediate-time power law behavior of the equal-time correlation modes depend on the mode momenta.

The observed behavior is reminiscent of a hydrodynamic regime connecting the exponential early-time and late-time regimes. One infers from Fig. 17 that at later times a strong deviation from the straight line occurs. For times around $x^0 \simeq 100/M_{\text{INIT}}$ the evolution is governed by neither a simple power nor exponential dependence. At sufficiently large times it approaches an exponential evolution towards thermal equilibrium (cf. Sect. 7.4).

7.3.3 *Strong interactions at intermediate times*

For higher n -point functions one can observe approximate power law behavior for certain intermediate time periods as well, however, the time evolution before the exponential late-time behavior can be rather complex. In Fig. 18 we show the effective four-point function $\lambda_{\text{eff}}(x^0; p = 0)$ for the above “tsunami” initial condition. We find that before times of about $x^0 \lesssim 300/M_{\text{INIT}}$ the drifting behavior is clearly non-exponential. For later times the evolution of $\lambda_{\text{eff}}(x^0; p)$ approaches an exponential time dependence with a characteristic zero mode rate $\gamma_{\lambda}^{(\text{therm})} \simeq 1.7 \times 10^{-3} M_{\text{INIT}}$. The thermalization time exceeds the characteristic damping time by more than an order of magnitude, similar to what has been observed above for the “quench” initial condition. This clear separation of scales happens despite the fact that the considered “tsunami” is weakly damped according to Eq. (7.7).

The effective coupling can, however, change substantially during the nonequilibrium evolution. From Fig. 18 we observe a large increase of $\lambda_{\text{eff}}(x^0; p = 0)$ in response to the “tsunami” initial condition. The system becomes effectively much stronger interacting for some time before it relaxes to equilibrium. For the considered initial condition the phenomenon of a strong interaction at intermediate times is restricted to the low momentum modes with $p \simeq 0$. For higher momenta we find that the effective coupling changes much less between the initial and the late-time value. One observes that the quick population of low momentum modes encountered in Fig. 15 goes along with a large effective coupling. Any estimate of the involved time scale needs to take into account the strong renormalization of the four-point

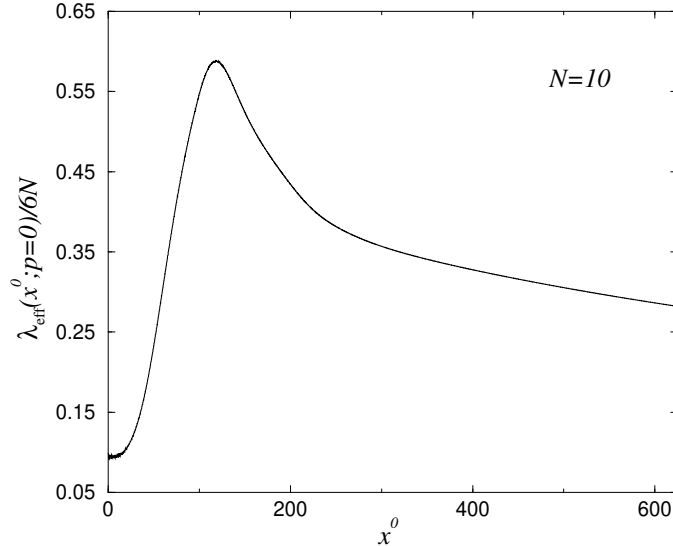


Figure 18: The effective four-point function $\lambda_{\text{eff}}(x^0; p)/6N$ at zero momentum for the “tsunami” employed in Fig. 15. The effective coupling for the zero momentum mode rises substantially at intermediate times before it approaches thermal equilibrium. For $x^0 \gtrsim 300/M_{\text{INIT}}$ the curve is very well approximated by an exponential behavior with rate $\gamma_{\lambda}^{(\text{therm})} \simeq 1.7 \times 10^{-3} M_{\text{INIT}}$.

function during the nonequilibrium evolution.

We stress that a simple exponential relaxation can never exhibit such a nontrivial behavior. The non-exponential drifting at intermediate times is an important phenomenon that separates the early-time and the late-time scales associated to exponential damping on the one hand and thermalization on the other hand. The overall time needed to reach thermal equilibrium crucially depends on this phenomenon and cannot be separated from it.

7.4 Late-time exponential thermalization

Independent of the detailed “quench” or “tsunami” initial conditions we find for sufficiently large times an exponential behavior to very good approximation. This is exemplified for the effective four-point function displayed in Figs. 13 and 14 after a “quench”. The latter figure verifies that after a certain time the correlation function follows closely the exponential fit for a large time range $\Delta x^0 = 1000/M_{\text{INIT}}$. A similar observation holds for

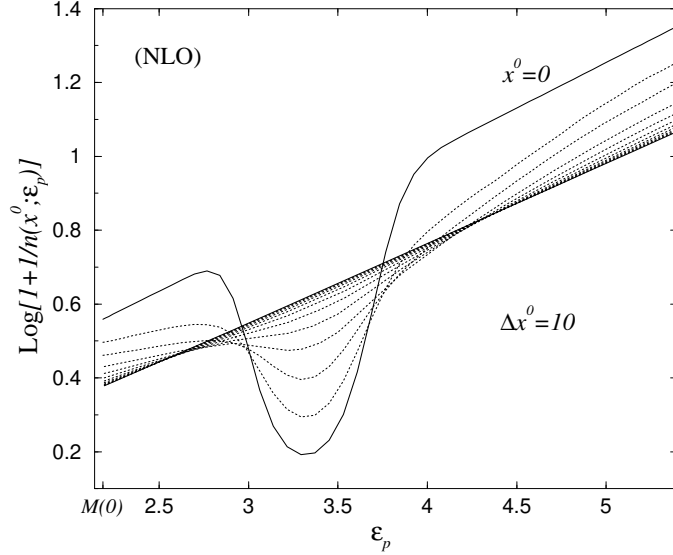


Figure 19: Effective particle number distribution for a “tsunami” in presence of a thermal background. The solid line shows the initial distribution which for low ($p \ll p_{\text{ts}}$) and for high ($p \gg p_{\text{ts}}$) momenta follows a Bose-Einstein distribution, i.e. $\ln[1+1/n(0; \epsilon_p)] \simeq \epsilon_p(0)/T_0$ with $T_0 = 4M_{\text{INIT}}$. At late times the nonthermal distribution equilibrates and approaches a straight line with inverse slope $T_{\text{EQ}} = 4.7 M_{\text{INIT}} > T_0$.

the “tsunami” employed in Fig. 18. In particular, for both types of initial conditions we find that the corresponding late-time scale exceeds the damping time scale by far, $\tau^{(\text{therm})} \gg \tau^{(\text{damp})}$. In other words, we observe a very efficient damping even for relatively weak coupling or, correspondingly, a slow thermalization.

To observe thermalization on a shorter time scale we discuss in the following a “tsunami” initial condition for a stronger coupling $\lambda/6N = 0.5 M_{\text{INIT}}^2$ (with $p_{\text{ts}} = 2.5M_{\text{INIT}}$, $\sigma = 0.25M_{\text{INIT}}$ and $\mathcal{A} = 4$ in Eq. (7.6)). In addition, we consider this peaked particle distribution in presence of a thermal background with initial “temperature” $T_0 = 4 M_{\text{INIT}}$.¹⁶ The initial particle number distribution can be inferred from the solid line of Fig. 19. Shown is the combination $\ln[1 + 1/n(x^0; p)]$ as a function of $\epsilon_p(x^0)$, where the effective particle number and mode energy are defined in Eqs. (7.8) and (7.3) respectively. If $n(\epsilon_p)$ strictly follows a Bose-Einstein distribution with

¹⁶The initial mass term given by Eq. (5.24) is $M(0) = 2.24M_{\text{INIT}}$.

temperature T then $\ln[1 + 1/n(x^0; p)] = \epsilon_p/T$. Correspondingly, from the solid line ($x^0 = 0$) in Fig. 19 one observes the initial “thermal background” as a straight line distorted by the nonthermal “tsunami” peak. In the interacting theory for $x^0 > 0$ the employed definitions for effective particle number and mode energy should allow for a characterization of the late-time thermal equilibrium in a similar way if a “quasi-particle” picture applies (cf. also the discussion in Ref. [5]).

Similar to the discussion of the initially weakly coupled “tsunami” in Sect. 7.3, one observes from Fig. 19 that the initial high occupation number in a small momentum range decays. More and more low momentum modes get excited and the particle distribution approaches a thermal shape. After rapid changes in $n(x^0; \epsilon_p)$ at early times the curves representing snapshots at equidistant time steps $\Delta x^0 = 10/M_{\text{INIT}}$ converge to a straight line to high accuracy with inverse slope $T_{\text{EQ}} = 4.7 M_{\text{INIT}} > T_0$. The asymptotic curve therefore corresponds precisely to what one expects of a thermally equilibrated “quasi-particle” distribution. We find that the asymptotic late-time result for the distribution is determined by the initial energy density and is insensitive to the details of the initial conditions (“thermal fixed point”). The latter observation has been explicitly demonstrated before in the three-loop approximation of the $2PI$ effective action in Ref. [12].

We emphasize again that thermalization or independence of the initial conditions cannot be observed in a strict sense because of time-reflection invariance (thermal equilibrium is invariant under time translation and bears no information about initial conditions). However, our results show that thermal equilibrium can be approached very closely without deviating from it over times of interest. Of course, the initial conditions for which thermalization can be observed in this sense have to comply with standard clustering requirements or not too large initial spread in energy¹⁷. It is important to note that starting from “first principles” in a time-reflection invariant, energy conserving description thermalization can only be achieved in the above sense: thermal equilibrium can be approached arbitrarily closely with time, indistinguishable for most practical purposes, however without reaching it on a fundamental level. This is a matter of principle and not a question of the employed approximation.

¹⁷Note that the energy and its moments are conserved quantities during the nonequilibrium time evolution. See also the detailed discussion in Ref. [34] for classical field theories.

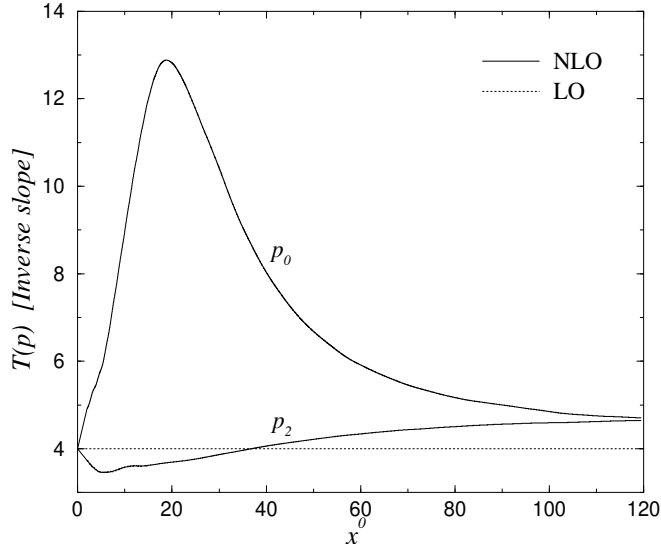


Figure 20: The time dependent inverse slope $T(x^0; p)$ of the distribution function as shown in Fig. 19. The function $T(x^0; p)$ is plotted for low momentum $p_0 \simeq 0$ and high momentum $p_2 \simeq 2p_{\text{ts}}$, where the slope of $\ln(1 + 1/n(x^0; \epsilon_p))$ is insensitive to small changes in ϵ_p at fixed x^0 and a characterization in terms of a “mode temperature” may be useful. At late times $T(x^0; p)$ becomes independent of momenta and the system can be described by a global value T_{EQ} .

7.4.1 Inverse slope parameter

In the following we consider the inverse slope of the effective particle number distribution as plotted in Fig. 19. For low momenta $p \ll p_{\text{ts}}$ or high momenta $p \gg p_{\text{ts}}$, where the slope of $\ln(1 + 1/n(x^0; \epsilon_p))$ is insensitive to small changes in ϵ_p at fixed x^0 , a characterization in terms of a “mode temperature” $T(x^0; p)$ may be useful — bearing in mind that away from thermal equilibrium this quantity has a precise meaning only in terms of the correlation functions employed in the definitions (7.3) and (7.8).

Fig. 20 shows the inverse slope $T(x^0; p)$ as a function of time for two momenta, $p_0 \simeq 0$ and $p_2 \simeq 2p_{\text{ts}}$ at NLO (solid line) and LO (dotted line). As pointed out above the particle number is conserved at LO and the initial nonthermal distribution is “frozen in”. Once scattering is taken into account at NLO the distribution evolves. One observes that for the low momentum modes $T(x^0; p)$ shoots up in response to the “tsunami” initial condition,

before dropping to the equilibrium value $T_{\text{EQ}} = 4.7 M_{\text{INIT}}$. While the low momentum modes get strongly “overheated” at intermediate times with respect to the thermal equilibrium value, one finds that the high momentum modes exhibit a small initial drop in $T(x^0; p)$ which then smoothly evolves. The population of the low lying modes involves a rapid change in the particle number distribution in which the inverse slope parameter overshoots the late-time value. Asymptotically the different “mode temperatures” converge.

It is interesting to observe that though the low momentum modes deviate at intermediate times much stronger from T_{EQ} than the high momentum ones, there is no substantial difference for the equilibration time as measured e.g. by the time at which they have approached T_{EQ} within 10 %. A similar observation can be made for the “quench” initial conditions discussed above where we do not see that some modes thermalize first.

8 Conclusion and outlook

The generating functional for $2PI$ Green’s functions provides a powerful technique for out-of-equilibrium physics. In combination with a $1/N$ expansion it yields a controlled nonperturbative description from “first principles” which is time-reversal invariant and energy conserving. The approach is not restricted to weak couplings or situations close to thermal equilibrium or to an effective description based on a separation of scales. With the present approach we have a quantitative method at hand which can deal with far-from-equilibrium processes, where the latter assumptions are typically not justified. An example is the possible strong renormalization of the effective four-point function at intermediate times for weak initial coupling (cf. Sect. 7.3.3), which stresses the fact that a clear separation of scales can be difficult to achieve away from equilibrium.

In this work we have studied two classes of initial conditions representing a “quench” and a “tsunami”, both in the weak $(2\pi\gamma_0^{(\text{damp})}/\epsilon_0 \ll 1)$ and the stronger coupling regime $(2\pi\gamma_0^{(\text{damp})}/\epsilon_0 \simeq \mathcal{O}(1))$. Independent of the details of the initial conditions we observe three qualitatively different time regimes, as summarized in Fig. 1. In particular, we find $\tau^{(\text{damp})} \ll \tau^{(\text{therm})}$ which emphasizes that the damping time cannot be identified with the thermalization time. It is possible to relate the damping rate to the “width” of the Wigner transformed spectral function ρ in the same way as discussed in Ref. [13], however, the thermalization rate cannot. Processes with nontrivial

momentum exchange are necessary for thermalization and are taken into account at NLO which includes off-shell effects¹⁸. On-shell particle number changing diagrams as the one in Fig. 5, which appears at next-to-next-to-leading order, can be important since they contain dynamics on which the bulk viscosity depends [2, 29].

We emphasize that scattering effects are crucial, even for rather early times. None of the features summarized in Fig. 1 are captured by the mean field type LO approximation which neglects direct scattering; no exponential damping (in particular, no suppression of correlations $F(x^0, 0; p)$ and $\rho(x^0, 0; p)$ with the initial time), no drifting and no thermalization can be observed in that case. The LO approximation typically breaks down after the first few oscillations and is approximately valid only for $x^0 \ll \tau^{(\text{damp})}$. However, for suitably time- or momentum-averaged quantities and not too strong couplings we find that the LO fixed point solution provides a rather accurate estimate up to times $x^0 \simeq \tau^{(\text{damp})}$. The latter observation agrees with what has been found for the corresponding classical field theory in Ref. [32].

We note that we are able to observe the same qualitative properties using the three-loop approximation of the $2PI$ effective action for $N = 1$ as employed in Refs. [12, 13]. Despite quantitative differences this points out that the qualitative properties discussed here do not depend on the detailed implementation of scattering and memory effects. In particular, this emphasizes the importance of the setting sun type diagram of Fig. 6. A detailed quantitative comparison is deferred to a separate publication which also discusses universality (independence of initial conditions) and parametric dependences of time scales [30].

There are many directions to pursue which are beyond the scope of the present work. With a more efficient numerics — the computations were done on a PC with unparallelized code — one can directly address similar problems in higher dimensions including the possibility of spontaneous symmetry breaking. This would allow for a quantitative quantum field theoretical study of the formation of disoriented chiral condensates in the context of heavy-ion collisions or of (p)reheating at the end of inflation in the early universe along the lines presented here. In the present form the time-

¹⁸In $1 + 1$ dimensions on-shell two-to-two scattering is constrained by the energy conservation relation such that it does not change the particle numbers for the involved momentum modes.

nonlocal scattering terms are difficult to estimate analytically. Though their numerical implementation is rather simple the calculations are time and memory consuming. However, one may expect that in higher dimensions both damping and thermalization become more efficient which reduces the need to follow the memory kernels to very large times. It is important to have a controlled, quantitative method which can serve as the basis for the development of approximation schemes which may allow to find reliable analytical solutions in limiting cases. The present techniques present a wealth of possibilities to study the applicability of standard phenomenological approaches. The range of validity of the classical Boltzmann equation or more sophisticated kinetic descriptions can be tested as well as other typical approximation schemes based on local equilibrium or linear response assumptions.

We emphasize that the current approach is not restricted to scalar fields though the presence of a small nonperturbative expansion parameter depends, of course, on the respective theory. It would be very desirable to extend the approach to include fermions and gauge fields.

Acknowledgements

I thank G. Aarts and J. Cox for collaboration on related work, and A. Jakovac, T. Prokopec and C. Wetterich for interesting discussions. I would like to thank W. Wetzel for support with computers.

References

- [1] J. Schwinger, *J. Math. Phys.* **2** (1961) 407; L. V. Keldysh, *Zh. Eksp. Teor. Fiz.* **47** (1964) 1515 [*Sov. Phys. JETP* **20** (1965) 1018].
- [2] For a digrammatic analysis in the context of a scalar theory see e.g. S. Jeon, *Phys. Rev.* **D52** (1995) 3591; S. Jeon, L. Yaffe, *Phys. Rev.* **D53** (1996) 5799.
- [3] For a review see D. Bödeker, *Nucl. Phys. Proc. Suppl.* **94** (2001) 61, and references therein.
- [4] Among the extensive literature on the leading-order approximation see e.g. F. Cooper, S. Habib, Y. Kluger, E. Mottola, J.P. Paz, P.R. Anderson, *Phys. Rev.* **D50** (1994) 2848; D. Boyanovsky, H.J. de Vega,

- R. Holman, D.S. Lee, A. Singh, Phys. Rev. **D51** (1995) 4419; S. Habib, Y. Kluger, E. Mottola, J.P. Paz, Phys. Rev. Lett. **76** (1996) 4660; D. Boyanovsky, H.J. de Vega, R. Holman, J.F.J. Salgado, Phys. Rev. **D54** (1996) 7570; F. Cooper, S. Habib, Y. Kluger, E. Mottola, Phys. Rev. **D55** (1997) 6471; J. Baacke, K. Heitmann, C. Pätzold, Phys. Rev. **D55** (1997) 2320; Phys. Rev. **D57** (1998) 6406; D. Boyanovsky, C. Destri, H.J. de Vega, R. Holman, J. Salgado, Phys. Rev. **D57** (1998) 7388; D. Boyanovsky, H. J. de Vega, R. Holman, J. Salgado, Phys. Rev. **D59** (1999) 125009; C. Destri, E. Manfredini, Phys. Rev. **D62** (2000) 025007; and references therein.
- [5] G. Aarts, J. Smit, Phys. Rev. **D61** (2000) 025002; M. Sallé, J. Smit, J. C. Vink, hep-ph/0012362, hep-ph/0012346. L. M. Bettencourt, K. Pao, J. G. Sanderson, hep-ph/0104210.
- [6] L.M.A. Bettencourt, C. Wetterich, Phys. Lett. **B430** (1998) 140;
- [7] B. Mihaila, J. F. Dawson, F. Cooper, Phys. Rev. **D56** (1997) 5400; L. M. Bettencourt, C. Wetterich, hep-ph/9805360; B. Mihaila, T. Athan, F. Cooper, J. Dawson, S. Habib, Phys. Rev. **D62** (2000) 125015; A. V. Ryzhov, L. G. Yaffe, Phys. Rev. **D62** (2000) 125003.
- [8] J. M. Cornwall, R. Jackiw, E. Tomboulis, Phys. Rev. **D10** (1974) 2428.
- [9] K. Chou, Z. Su, B. Hao, L. Yu, Phys. Rept. **118** (1985) 1.
- [10] E. Calzetta, B. L. Hu, Phys. Rev. **D37** (1988) 2878.
- [11] See also J.M. Luttinger, J.C. Ward, Phys. Rev. **118** (1960) 1417; G. Baym, Phys. Rev. **127** (1962) 1391; B. Vanderheyden, G. Baym, hep-ph/0002291.
- [12] J. Berges, J. Cox, hep-ph/0006160.
- [13] G. Aarts, J. Berges, hep-ph/0103049.
- [14] L.P. Kadanoff, G. Baym, “Quantum Statistical Mechanics”, Benjamin, New York (1962).
- [15] P. Danielewicz, Ann. Phys. **152** (1984) 239; **197** (1990) 154;
- [16] S. Mrowczynski, P. Danielewicz, Nucl. Phys. **B342** (1990) 345;

- [17] S. Mrowczynski, U. Heinz, *Annals Phys.* **229** (1994) 1.
- [18] J. Blaizot, E. Iancu, hep-ph/0101103.
- [19] Y. B. Ivanov, J. Knoll, D. N. Voskresensky, *Nucl. Phys.* **A672** (2000) 313; S. Leupold, *Nucl. Phys.* **A672** (2000) 475.
- [20] M. Joyce, K. Kainulainen, T. Prokopec, *Phys. Lett.* **B474** (2000) 402.
- [21] J. Berges, K. Rajagopal, *Nucl. Phys.* **B538** (1999) 215; M. A. Halasz, A. D. Jackson, R. E. Shrock, M. A. Stephanov, J. J. Verbaarschot, *Phys. Rev.* **D58** (1998) 096007.
- [22] B. Mihaila, F. Cooper, J. F. Dawson, *Phys. Rev.* **D63** (2001) 096003.
- [23] K. Rajagopal, F. Wilczek, *Nucl. Phys.* **B404** (1993) 577.
- [24] R.D. Pisarski, hep-ph/9710370; D. Boyanovsky, H.J. de Vega, R. Holman, S.P. Kumar, R.D. Pisarski, *Phys. Rev.* **D57** (1998) 3653.
- [25] L. McLerran, R. Venugopalan, *Phys. Rev.* **D49** (1994) 2233; (1994) 3352; for a recent review see e.g. L. McLerran, hep-ph/0104285.
- [26] R.D. Pisarski, private communication.
- [27] P. Arnold, L. G. Yaffe, *Phys. Rev.* **D57** (1998) 1178.
- [28] F. Cooper, S. Habib, Y. Kluger, E. Mottola, *Phys. Rev.* **D55** (1997) 6471.
- [29] E.A. Calzetta, B.L. Hu, S.A. Ramsey, *Phys. Rev.* **D61** (2000) 125013.
- [30] G. Aarts, J. Berges, in preparation.
- [31] C. Wetterich, *Phys. Rev.* **E56** (1997) 2687 ; *Phys. Rev. Lett.* **78** (1997) 3598.
- [32] G. Aarts, G.F. Bonini, C. Wetterich, *Phys. Rev.* **D63** (2001) 025012.
- [33] For a recent review on this subject see J. Berges, N. Tetradis, C. Wetterich, appears in *Phys. Rept.* (hep-ph/0005122).
- [34] G. Aarts, G. F. Bonini, C. Wetterich, *Nucl. Phys.* **B587** (2000) 403 .